

**USING SUBJECT-SPECIFIC MUSCLE PARAMETERS TO COMPARE
MUSCLE FORCES AND ACTIVATION BETWEEN AN EMG-DRIVEN AND
OPENSIM MUSCULOSKELETAL MODEL**

by

David Olchowski

A thesis submitted to the Faculty of the University of Delaware in partial fulfillment of the requirements for the degree of Master of Science in Mechanical Engineering

Fall 2010

© 2010 David Olchowski
All Rights Reserved

**USING SUBJECT-SPECIFIC MUSCLE PARAMETERS TO COMPARE
MUSCLE FORCES AND ACTIVATION BETWEEN AN EMG-DRIVEN AND
OPENSIM MUSCULOSKELETAL MODEL**

by
David Olchowski

Approved: _____
Thomas S. Buchanan, Ph.D.
Professor in charge of thesis on behalf of the Advisory Committee

Approved: _____
Anette M. Karlsson, Ph.D.
Chair of the Department of Mechanical Engineering

Approved: _____
Michael J. Chajes, Ph.D.
Dean of the College of Engineering

Approved: _____
Charles G. Riordan, Ph.D.
Vice Provost for Graduate and Professional Education

ACKNOWLEDGMENTS

I am extremely thankful and feel so lucky to have had the opportunity to work with two great advisors, Dr. Thomas S. Buchanan and Dr. Jill S. Higginson. Both have been tremendously helpful throughout this process, whether with questions or guidance along the way. I feel honored to have been able to work under two people who are tremendously knowledgeable and enthusiastic about their research.

I want to thank my committee members Dr. Buchanan, Dr. Higginson, and Dr. Manal. Their continued support throughout my time at the University of Delaware has meant so much, and I cannot thank them enough.

In addition to my advisors and committee members, I have benefited greatly from daily discussions with all of my lab members, including Andy Kubinski, Anantharaman Gopalakrishnan, Chris Henderson, Xiao Ming, Chris Richards, Ben Roewer, Steve Suydam, Nicole Zahradka, Elisa Schrank, Shridhar Shah, and Emily Gardinier. I would also like to especially thank John Ramsay, Nils Hakansson, Brian Knarr, and Qi Shao for all their help with OpenSim, the EMG-driven model, and data collections. I would not have been able to finish this thesis without their unending support and assistance.

Finally, I would like to thank all of my family and friends. I have had a tremendous experience at the University of Delaware over the past three years and I could not imagine going through it all without them. I have grown both academically and personally, and the love from all has shaped who I am today. Thank you again for everything.

This study was funded by NIH NS 055383 and NIH AR 046386, UD's
ME Teaching Assistantship and ME Research Assistantship.

David Olchowski

Newark, DE

August, 2010

TABLE OF CONTENTS

LIST OF TABLES	vii
LIST OF FIGURES	viii
ABSTRACT	ix
Chapter	
1 INTRODUCTION	1
1.1 Focus of the Thesis	2
1.1.1 Aim 1	3
1.1.2 Aim 2	3
1.2 Significance of Research	4
1.3 Thesis Structure	5
2 BACKGROUND	6
2.1 Musculoskeletal Modeling	6
2.1.1 Static Optimization	7
2.1.2 Dynamic Optimization	8
2.1.3 EMG-to-force Models	9
2.2 The EMG-driven Model	10
2.2.1 Muscle Activation Dynamics	12
2.2.2 Muscle Contraction Dynamics	16
2.2.2.1 Active and Passive Force-Length Relationship	17
2.2.2.2 Force-Velocity Relationship	20
2.2.2.3 Damping Component	21
2.2.2.4 Pennation Angle	22
2.2.2.5 Tendon Force Relationship	22
2.2.2.6 Maximum Isometric Force Strength Factors	23

2.2.3 Muscle Parameters & Model Optimization	24
2.3 OpenSim Model.....	26
2.3.1 Model Scaling.....	27
2.3.2 Inverse Kinematics	27
2.3.3 Reduced Residual Algorithm.....	28
2.3.4 Computed Muscle Control	30
2.4 Summary.....	33
3 METHODS.....	35
3.1 Experimental Data	35
3.1.1 Walking Trials	35
3.1.2 Electromyography Data	35
3.1.3 Maximum Voluntary Contraction Trials	36
3.1.4 Data Processing	36
3.2 The EMG-driven Model	37
3.2.1 Model Structure	37
3.2.2 Model Inputs.....	38
3.3 OpenSim Simulation	40
3.3.1 Model Compatibility.....	41
3.3.2 Scaling, Inverse Kinematics, & Inverse Dynamics.....	41
3.3.3 Reduced Residual Algorithm & Computed Muscle Control.....	43
3.4 Model Comparison and Calculations	44
4 RESULTS	46
4.1 The EMG-driven Model	46
4.1.1 Model Calibration.....	46
4.1.2 Optimized Parameters	48
4.1.3 Activation and Force for the Biarticular Gastrocnemius	50

4.2 Muscle Activation & Force Comparison for OpenSim & EMG-driven Models.....	51
4.2.1 Knee Extensors	51
4.2.2 Knee Flexors.....	55
4.2.3 Ankle Plantar Flexors & Dorsiflexors.....	57
4.2.4 Net Joint Forces.....	60
5 DISCUSSION.....	62
5.1 Determination of Optimized Muscle Parameters	63
5.2 Generic Vs. Optimized Muscle Parameters in OpenSim	65
5.2.1 Optimal Fiber Length	66
5.2.2 Tendon Slack Length.....	68
5.2.3 Maximum Isometric Force	69
5.2.4 Summary.....	70
5.3 EMG-driven Model Vs. Optimized OpenSim Model	71
5.3.1 Activation Dynamics	71
5.3.2 Contraction Dynamics	72
5.3.3 Cost Function.....	73
5.3.4 Summary.....	74
5.4 Net Joint Forces	75
5.5 Conclusions	77
5.6 Limitations.....	79
5.7 Future Work.....	81
REFERENCES	83

LIST OF TABLES

3.1	The physiological ranges between which the global and muscle-specific parameters can be optimized.....	40
3.2	OpenSim generic model initial values.....	42
3.3	Weight factors for scaling and IK.....	43
4.1	Individual and averaged r^2 , RMS, and normalized peak-to-peak RMS error values for the EMG-driven forward dynamic calibration of joint moments.....	47
4.2	Average (OpenSim) scaled and (EMG-driven model) optimized values for all subjects with percent differences for OFL and TSL.....	49
4.3	Generic (OpenSim) and averaged optimized MF values from all subjects based on G_f , G_e from the EMG-driven model.....	50
4.4	Peak values and percent differences of the MG, LG forces and activations from the knee and ankle EMG-driven models	51
4.5	Muscle activation ratios using average area under curve from the Trapezoidal Rule	52
4.6	Muscle force ratios using average area under curve from the Trapezoidal Rule	54
4.7	r^2 , RMS, and normalized peak-to-peak RMS error values for the net knee and ankle force for all subjects.....	61

LIST OF FIGURES

2.1	Flowchart of the hybrid forward and inverse dynamics muscle force model.....	11
2.2	The transformation from raw EMG to muscle activation.....	13
2.3	Graph defining the one-parameter nonlinearization of neural activation to muscle activation.....	15
2.4	Hill-type model schematics of the muscle-tendon unit and the muscle fiber	17
2.5	Normalized force-length curve.....	19
2.6	OpenSim model schematic showing the steps of musculoskeletal analysis.....	27
2.7	Computed Muscle Control algorithm.....	31
4.1	Average calibrated forward dynamics moment from the EMG-driven model.....	47
4.2	Muscle activations of the knee extensors for subject 1	53
4.3	Muscle forces of the knee extensors for subject 1	54
4.4	Muscle activations of the knee flexors for subject 1	56
4.5	Muscle forces of the knee flexors for subject 1	57
4.6	Activations of the ankle muscles for subject 1	58
4.7	Forces of the ankle muscles for subject 1	59
4.8	Net knee and ankle joint forces for subject 1	60

5.1	Normalized fiber length for the Sol and LG during stance phase for subject 1.....	67
-----	--	----

ABSTRACT

Experimental gait analysis was developed to analyze and calculate mechanical aspects such as joint kinetics and kinematics to understand the characteristics that lead to human walking. Unfortunately, gait analysis is limited because it alone cannot determine individual, in vivo muscle function. Redundant systems are created from multiple muscles spanning one joint, thus eliminating the possibility to directly calculate muscle activity. The recent use of musculoskeletal modeling has allowed researchers to extend the functionality of gait analysis, predict individual muscle activity and forces, and gain insight to the underlying neuromuscular function.

Many different optimization approaches with varying degrees of complexity exist to estimate individual muscle forces and activation. Previous studies have used electromyograms (EMG) to derive subject-specific muscle parameters that match inverse dynamics, while others use a generic model and redistribute muscle forces across synergistic muscles based on a particular cost function. Because generic musculoskeletal models are limited by their lack of specificity, we hoped to include subject-specific muscle parameters that would lead to improved force predictions. Prior sensitivity studies have determined the effect of altering one parameter within a

specified range and calculating the difference in forces. However, to date, a global set of muscle parameters has not been implemented within a forward dynamic simulation.

In this thesis, we compared forward simulations of healthy subjects using generically scaled and subject-specific muscle parameters. Specifically, differences in muscle force and activation using optimized values of maximum isometric force, optimal fiber length, and tendon slack length were examined. An EMG-driven model was used as a means to determine subject-specific muscle parameters. OpenSim, an open-source software, was used to provide a computationally efficient forward simulation based on a computed muscle control algorithm. Output forces from subject-specific EMG-driven and OpenSim forward dynamic simulation models were compared to determine differences between the two fundamentally contrasting models.

The EMG-driven model matched the experimental inverse dynamic joint moments well with average r^2 values of 0.924 and 0.954 for the knee and ankle, respectively, giving confidence that the optimized muscle parameters are indicative of true in vivo values and provide good predictive ability for novel tasks. OpenSim forward dynamic simulations produced lower average activations with optimized subject-specific parameters than generically scaled parameters for all muscles except the BFLH.

Average ratios of muscle force from the scaled to optimized OpenSim models were below 1.0 for all muscles except the Sol, indicating larger optimized force values. Because both models apply the same cost function, differences in force are

due solely to changes in muscle parameters. Similarly, a comparison of the muscle forces from the EMG-driven to optimized OpenSim models revealed ratios below 1.0 for all muscles except the Sol. Fundamental differences in the model cost functions and their calculation of forces are responsible for these differences as the muscle physiology between the two models is held constant.

Although the models showed varying individual muscle forces, it is still encouraging that similar net joint forces were produced at both joints, and in particular, the ankle. r^2 values for the net ankle forces ranged between 0.917 and 0.999. Timing and magnitude were also similar for the ankle with differences in peak values only ranging from 24 to 592N.

This thesis examined the global use of subject-specific parameters within an EMG-driven and OpenSim forward dynamic model. While an exact cause-and-effect relationship is difficult to determine for each particular change in a muscle parameter, we believe that the use of subject-specific parameters will improve the utility of forward dynamic simulations and can be extended to gain insight into the deficiencies in neuromuscular function of pathologic patients.

Chapter 1

INTRODUCTION

Although common, walking requires complex neural and muscular coordination. To gain a better perspective of the task, gait analysis has been used to understand movement of the lower limbs (Buchanan & Shreeve, 1996; Manal et al., 2002, Seireg & Arvikar, 1973, Piazza & Delp, 1996; Glitsch & Bauman, 1997; Kaufman et al., 1991; Crowninshield & Brand, 1981; Lloyd & Besier, 2003; Heintz & Gutierrez-Farewik, 2007; Neptune & Hull, 1998; Neptune et al., 2001; Anderson & Pandy, 2001a; Neptune, 1999). Motion capture, force plates, and electrodes were implemented to determine and calculate gait kinematics, kinetics, ground contact forces, and electromyographic signals. While much can be learned about joint and segment movements, gait analysis is limited by the fact that it cannot provide information about individual muscle activity. Redundant systems are created when multiple muscles span a joint, thus making it impossible to directly calculate individual muscle forces. Additionally, walking is a highly coordinated movement, meaning the motion of any one joint will affect another.

Computer based simulations offer a new approach to solve the problem of the redundant system. Cost functions can be used to distribute forces across synergistic muscles and give insight into how the neuromuscular system activates muscles. While

cost functions for activities such as maximal jumping height are task-specific (i.e. maximize jump height), the cost function for human gait is not well established. Researchers have applied various cost functions minimizing muscle stresses (Glitsch & Bauman, 1997; Pedotti et al., 1978; Kaufman et al., 1991), joint compressive force (Bean et al., 1988), metabolic energy (Anderson & Pandy, 2001a; Liu et al., 2006), and endurance (Crowninshield & Brand, 1981) in human walking.

Three prominent methods exist in muscle modeling: static optimization, dynamic optimization, and EMG-to-force. Each incorporates some variation of input kinematics, kinetics, and muscle physiology to estimate muscle activity. Results can lead to greater understanding of muscular coordination and highlight wide-ranging possibilities to clinical approaches to sports injury prevention, pathological gait, and rehabilitation programs.

1.1 Focus of the Thesis

Computer based simulations of human gait typically begin with a musculoskeletal model consisting of the segments of interest. Accurate muscular physiology is critical to the quality of the resulting output. OpenSim, an open-source simulation software, uses muscle parameters from previously reported cadaver data and scales them according to subject dimensions. In this thesis, we examined differences in forces and activations seen with the use of subject-specific parameters from an EMG-driven model. The specific aims of the thesis were:

1.1.1 Aim 1: Determine the difference in muscle activation and force between an OpenSim forward dynamic simulation based on generically scaled and optimized subject-specific parameters

A generic model was built to reproduce self-selected walking data from three healthy subjects. An EMG-driven model was run to determine optimized muscle parameters. Subject-specific values of maximum isometric force, optimal fiber length, and tendon slack length for 12 knee and ankle muscles were input into the OpenSim model in place of generic values. Two forward dynamic simulations were implemented based on identical kinematic and kinetic data with muscle parameters the sole difference. We compared output activations and forces from a computed muscle control algorithm.

1.1.2 Aim 2: Determine the difference in muscle force between an EMG-driven model and an OpenSim forward dynamic simulation based on subject-specific parameters

While the EMG-driven and OpenSim models have fundamentally different approaches to the estimation of muscle activity, both determine values for individual muscle force using a Hill-type model. Since the muscle parameters used in the subject-specific OpenSim model were determined using the EMG-driven model, both

have identical muscle parameters. We compared the output force for the muscles spanning the knee and ankle joints.

1.2 Significance of Research

Forward dynamic simulation presents an opportunity for researchers to better understand neural and muscular coordination. Many factors determine the quality of the result such as computational time, experimental data, model complexity, and muscle physiology. In this thesis we looked at the effect of subject-specific parameters, specifically maximum isometric force, optimal fiber length, and tendon slack length on predictions of muscle activation and force.

Previous forward dynamic simulations have used generic models to simulate experimental data. Other studies have looked at the sensitivity of perturbing a single parameter and calculating the resulting differences in muscle force (Xiao et al., In press). Here, we adjusted a total of 36 parameters across 12 knee and ankle joint muscles. Because these values were optimized to particular subjects, we believe that our results can give greater insight into the underlying neuromuscular function in not only healthy subjects, but pathologic patients as well. Clinically, this information can be used to tailor rehabilitation programs to target particular deficiencies and improve the quality of life of these individuals.

1.3 Structure of Thesis

The next chapter reviews previous studies on the various modeling approaches, describing in detail the EMG-driven and OpenSim models. Chapter 3 describes the particular methods used in the study. Chapter 4 analyzes the results of the activation and force comparisons between the models. Chapter 5 discusses the major findings of the thesis, the significance of the results, and possible future directions.

Chapter 2

BACKGROUND

2.1 Musculoskeletal Modeling

While studies measuring muscle force directly have been performed (Komi et al., 1987; Komi, 1990; Gregor et al., 1991; Komi, 1992), their invasive nature and limited applicability has encouraged researchers to investigate other, less invasive methods. Many approaches exist to model muscles with the intention of obtaining individual muscle forces. A.F. Huxley developed the cross-bridge theory which details the physiological structure of muscle (Huxley, 1958). Although this has been implemented successfully (Zahalak, 1986; Zahalak, 2000), from a biomechanist's point of view, models with this level of complexity are not needed for the estimation of muscle forces. Huxley's biophysical model, and others like it, are also very computationally expensive.

Muscle contractions, force development, and resulting body movements can instead be viewed on a more phenomenological basis. A.V. Hill developed a model of the behavior of muscle from a broader perspective with defined contractile conditions based on empirical data (Hill, 1938). The primary problem involved in accurately estimating individual muscle forces is that numerous muscles span any one joint,

creating a redundant system. There are an infinite number of muscle force combinations that can sum to the experimentally measured joint moment.

Optimization of a cost function can give insight into how the neuromuscular system activates muscles during particular tasks. Many studies using cost functions minimize muscle stresses (Glitsch & Bauman, 1997; Pedotti et al., 1978; Kaufman et al., 1991) while others have minimized joint compressive force (Bean et al. 1988) or muscle endurance (Crowninshield & Brand, 1981). Computer based simulations provide an ability to estimate muscle forces based on a particular cost function. A wide variety of approaches with varying levels of complexity have been presented to estimate muscle force (Buchanan & Shreeve, 1996; Manal et al., 2002, Seireg & Arvikar, 1973, Piazza & Delp, 1996; Glitsch & Bauman, 1997; Kaufman et al., 1991; Crowninshield & Brand, 1981; Lloyd & Besier, 2003; Heintz & Gutierrez-Farewik, 2007; Neptune & Hull, 1998; Neptune et al., 2001; Anderson & Pandy, 2001a; Neptune, 1999). Three main simulation methods exist: static optimization, dynamic optimization, and EMG-to-force models.

2.1.1 Static Optimization

Static optimization involves applying a cost function to distribute muscle forces from a joint moment calculated at each user defined time step. Joint moments are determined from the use of experimental data and an inverse dynamic simulation. The particular cost function then decomposes the joint moment into individual muscle

moments from which forces can be determined through the use of moment arms. Because the joint moment is calculated at each time step, as opposed to over an entire range of motion, computational time is minimal. Several studies have shown promising results with static optimization (Anderson & Pandy, 2001b; Anderson & Pandy, 2003; Crowninshield & Brand, 1981).

Several limitations, however, still exist with the use of static optimization. The inverse dynamic inputs are the experimental data, ground reaction forces, and segment anthropometry, making the accuracy of joint moments highly correlated with the accuracy of the collected data (Davy & Audu, 1987). In addition, the time-independent nature of static optimization does not allow for insight into the individual muscle contributions to the acceleration of segments because of the lack of a full set of dynamic equations (Zajac, 1993). Importantly, muscle physiology is difficult to include because parameters are continuously changing between time steps. Dynamic models which could account for an entire movement help minimize these limitations.

2.1.2 Dynamic Optimization

Forward dynamic simulation determines body motion (joint accelerations, velocities, and angles) based on input muscle activations. Initial muscle activations are predicted based on underlying muscle physiology and the resulting motion is compared with the experimental motion. The activations are iteratively updated until the particular cost function, such as minimizing metabolic energy (Anderson & Pandy,

2001a) or minimizing differences between experimental and simulated motions (Neptune et al., 2001; Zajac et al., 2003; Higginson et al., 2006), converges to optimal values. While studies have shown forward simulations are capable of analyzing muscle function during gait (Zajac et al., 2003; Anderson & Pandy, 2003; Liu et al., 2006; Neptune et al., 2001), implementation of these models are computationally expensive due to the fact that the model is optimized over the entire movement. Recently, Delp et al. (2007) developed an open-source software called OpenSim that combines the complexity of forward simulation with the computational speed of static optimization. This model will be described in further detail later.

2.1.3 EMG-to-force Models

Electromyograms (EMG) can highlight critical information about how the central nervous system activates muscles. Models using this data have estimated moments of the knee (Lloyd & Buchanan, 1996; Lloyd & Besier 2003), lower back (Thelen, 1994), elbow (Manal et al., 2002), and wrist (Buchanan et al., 1993). In the EMG-driven model described here, musculoskeletal parameters are tuned to individual subjects and estimated muscle forces can be determined by a hybrid forward and inverse dynamic optimization method. After the parameters are tuned, the inverse dynamics portion can be eliminated and the forward dynamics can then be used to predict muscle forces in novel tasks.

2.2 The EMG-driven Model

The EMG driven model incorporates both inverse and forward dynamic approaches. First, during a particular trial, position data from markers and external forces (i.e. ground reaction forces) are collected. Joint angles are calculated and differentiated to obtain angular velocities and accelerations. Using a scaled model and rigid body dynamics, joint moments can be estimated. Because multiple muscles cross each joint, it is challenging to estimate individual muscle forces accurately. With defined musculoskeletal geometry and an optimization cost function this can be overcome. However, for the purposes of the hybrid EMG model, our calculations will stop at the joint moment. The inverse dynamic joint moment is then used to calibrate the forward dynamic moment. Musculoskeletal parameters are perturbed and the forward dynamic loop is rerun until the difference between the two joint moments is minimized (Figure 2.1).

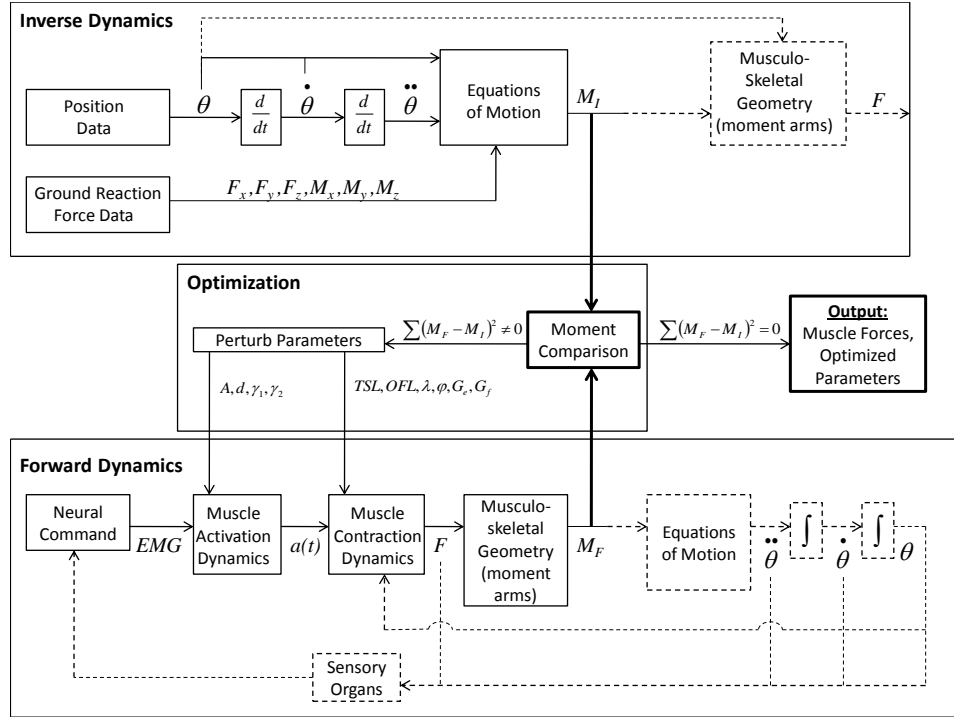


Figure 2.1: Flowchart of the hybrid forward and inverse dynamics muscle force model. The operations marked by dashed lines indicate portions of the traditional forward and inverse dynamic loops that are not performed in the hybrid method. Legend: θ (and derivatives) = joint angle, joint angular velocity, joint angular acceleration; M_I = total inverse dynamic joint moment; M_F = total forward dynamic joint moment; F = muscle forces; EMG = electromyograms; $a(t)$ = muscle activation; A = shape factor; d = electromechanical delay; γ_1, γ_2 = recursive filter parameters; TSL = tendon slack length; OFL = optimal fiber length; λ = force-length skew coefficient; φ = pennation angle; G_f, G_e = flexor and extensor gain factors; $F_x, F_y, F_z, M_x, M_y, M_z$ = ground reaction forces and moments in all three directions (adapted from Bassett et al. 2006).

Conversely, the forward dynamics begins with neural command which is estimated through the use of EMG. Since it is difficult to compare EMG signals between muscles because of extraneous factors such as the amount of tissue between

an electrode and muscle and the electrode's placement, muscle activation dynamics is used to transform the EMG to dimensionless, time-varying muscle activations with values varying between zero and one. Muscle contraction dynamics then determines individual muscle forces from the muscle activations (Buchanan et al. 2004). From muscle forces and moment arms, the joint moment can easily be calculated (Figure 2.1). Equations of motion, inertial properties, and external forces and moments can lead to joint angles, velocities, and accelerations, but again, we will stop at the calculation of the joint moment to calibrate the model.

2.2.1 Muscle Activation Dynamics

Muscle activation dynamics begins with EMG from individual muscles as inputs. EMG is the electrical signal, measured in volts, created from a contracting muscle. The first step in transforming EMG to activation is to remove the low frequency noise caused by skin or electrode movement. A high-pass filter is applied in the 5-30 Hz range (Buchanan et al., 2004). The signal is then rectified by taking the absolute value of all points (Figure 2.2). Next, the signal is smoothed by using a low-pass filter to eliminate any interference. Typical low-pass filters used are in the range 3-10 Hz (Buchanan et al., 2004). Lastly, the signal is normalized to maximum voluntary contraction (MVC) values. This is done in an effort to allow comparisons between muscles. The resulting normalized, rectified, and filtered values, $e(t)$, will then range from zero (no activity) to one (full activity).

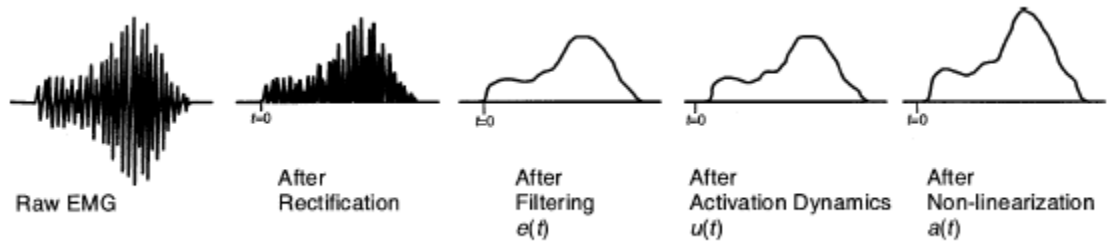


Figure 2.2: The transformation from raw EMG to muscle activation, $a(t)$, during muscle activation dynamics (as seen in Buchanan et al. 2004).

Although EMG measures electrical activity that eventually leads to muscle force, the process is not instantaneous. A time delay, unique to each muscle, can account for this gap. Different relationships have been used to model the transformation. Milner-Brown et al. (1973) originally used a second-order linear differential equation. Over time, other approaches have been used such as a first-order linear differential relationship (Zajac, 1989) and a first-order recursive filter (Thelen, 1994). Our model incorporates a recursive filter based on a discretized form of a second-order differential equation (Lloyd & Besier, 2003; Buchanan et al., 2004) which models the neural activation, $u(t)$, as

$$u(t) = \alpha \cdot e(t - d) - \beta_1 \cdot u(t - 1) - \beta_2 \cdot u(t - 2) \quad (1)$$

where d is the electromechanical delay, and α , β_1 , and β_2 are coefficients defining the second-order dynamics. Values for the electromechanical delay have been shown to range between 10-100 msec (Corcos et al., 1992). Buchanan (2004) showed that the following conditions must hold true for the recursive filter to be stable

$$\beta_1 = \gamma_1 + \gamma_2 \quad (2)$$

$$\beta_2 = \gamma_1 \cdot \gamma_2 \quad (3)$$

$$|\gamma_1| < 1 \quad (4)$$

$$|\gamma_2| < 1 \quad (5)$$

$$\alpha - \beta_1 - \beta_2 = 1 \quad (6)$$

As seen in equation (1), neural activation is dependent on the two previous values of $u(t)$. In order for the gain not to exceed 1, equation (6) is used to constrain these parameters. From equations (2)-(6), it can be seen that the only parameters necessary to transform $e(t)$ to $u(t)$ are d , γ_1 , and γ_2 . These are obtained using an optimization algorithm described later.

While researchers have used neural activation, $u(t)$, to estimate muscle activation, $a(t)$, Woods & Bigland-Ritchie (1983) showed that in many muscles a nonlinear relationship exists between force and neural activation. Their study showed that for activation values up to approximately 30%, the relationship was nonlinear, and linear thereafter. Manal and Buchanan (2003) accounted for this by developing a model that used a logarithmic function for lower activation values:

$$\begin{aligned}
 a(t) &= d \ln(cu(t) + 1) & 0 \leq u(t) < 0.3085 \\
 a(t) &= mu(t) + b & 0.3085 \leq u(t) < 1
 \end{aligned}
 \tag{7}$$

The coefficients b , c , d , and m can all be determined from a single parameter, A (Figure 2.3).

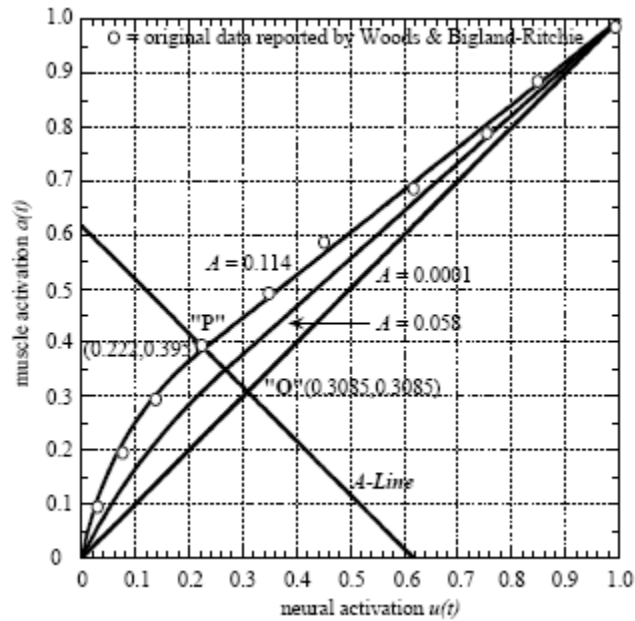


Figure 2.3: Graph defining the one-parameter nonlinearization of neural activation to muscle activation (Manal & Buchanan, 2003). Circles on the graph represent data Woods & Bigland-Ritchie (1983).

The values of P and Q along the ‘ A -line’ help define the shape factor A . The shorter the distance between P and Q , the smaller the value of A will be. An A value of virtually zero ($A = .0001$ on Figure 2.3) characterizes a linear relationship between neural activation and muscle activation. The experimental data from Woods &

Bigland-Ritchie (2003) on the graph is used to show a similar relationship between their results and the one-parameter neural activation to muscle activation model (Manal & Buchanan, 2003)

2.2.2 Muscle Contraction Dynamics

The next step in the EMG-driven model is muscle contraction dynamics, in which individual muscle forces are determined from muscle activations. Hill-type models, which typically require only one differential equation per muscle, are used instead of the more computationally expensive Huxley model.

In the Hill-type model, the muscle is in series with the viscoelastic tendon (Figure 2.4). The relationship is represented mathematically by,

$$F_t = F_m^o \left[\tilde{F}_A(\tilde{l}_m) \cdot \tilde{F}_V(\tilde{v}_m) \cdot a(t) + \tilde{F}_P(\tilde{l}_m) + b_m \cdot \tilde{v}_m \right] \cdot \cos(\varphi) \quad (8)$$

where F_t is the tendon force, F_m^o is the maximum isometric force, \tilde{F}_A , \tilde{F}_V , and \tilde{F}_P are the normalized active, velocity-dependent, and passive forces, respectively, \tilde{l}_m is the normalized muscle fiber length, \tilde{v}_m is the normalized muscle fiber velocity, $a(t)$ is the time-dependent muscle activation, b_m is the damping factor, and φ is the pennation angle (Bassett et al., 2006). By using normalized values of forces, length, and

velocity, we are able to use similar force-length and force-velocity relationships for all muscles.

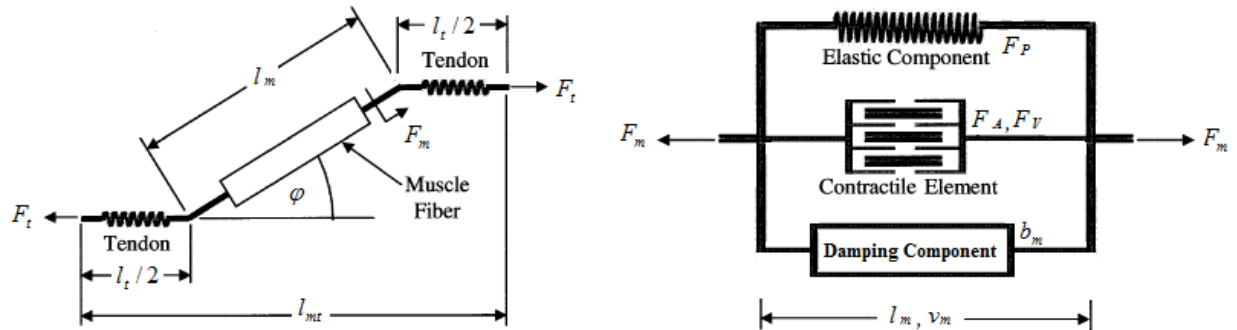


Figure 2.4: Hill-type model schematics of the muscle-tendon unit and the muscle fiber. The tendon is in series with the muscle fiber relative to the pennation angle, ϕ . The tendon on either side of the muscle fiber, $l_t/2$, is half the total tendon length. The muscle fiber consists of three elements in parallel. The elastic component is described by the passive force-length relationship and gives F_P . The contractile element (sarcomeres) is described by the active force-length and force-velocity relationships and gives F_A and F_V . The damping component gives b_m (adapted from Bassett et al., 2006; Buchanan et al. 2004).

2.2.2.1 Active and Passive Force-Length Relationship

Active force in muscle is generated through a motor unit, the sarcomere, while passive force acts in resistance to the muscle fiber when stretched beyond its resting length. The sarcomere consists of two overlapping components: the actin and myosin filaments (Figure 2.5, contractile element). As the muscle contracts, the myosin (thick

bands) pulls the actin (outer lines) (Lieber et al., 1994). When the sarcomere is at its optimal overlap, the resulting fiber length is called the optimal fiber length, l_m^o , and the muscle is at its maximum force generating potential. Above and below this optimal overlap, the force will drop off.

By normalizing certain variables (force to maximum isometric force and length to optimal fiber length, in this case), a dimensionless force-length relationship can be used for all muscles. This complex relationship has more recently been modeled as a second order polynomial (Woittiez et al., 1984), however it was best represented originally by Gordon et al. (1966). Figure 2.5 shows normalized active, passive, and total muscle force. The active force rises and falls rapidly, and plateaus for a short period in the middle of muscle contraction. When muscle activation is 1.0, the active force curve peaks at its optimal fiber length. Huijing (1996) showed that with lower values of activation, the optimal fiber length increases. Lloyd and Besier (2003) accounted for this with a force-length skew coefficient, λ , of .15, meaning the optimal fiber length at zero activation is 15% percent longer than the optimal fiber length at an activation of 1.0. Mathematically, they showed the coupling between muscle activation and optimal fiber length as,

$$l_m^o(t) = l_m^o(\lambda(1 - a(t)) + 1). \quad (9)$$

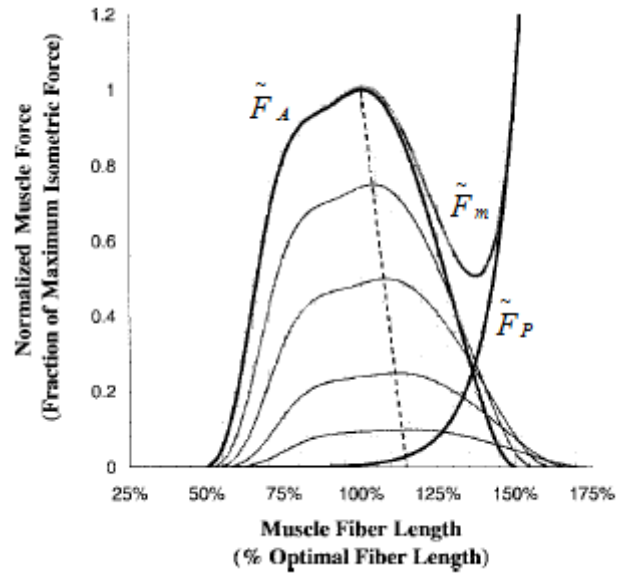


Figure 2.5: Normalized force-length curve. Bold lines represent normalized active, passive, and total muscle force. The bold active force line is when muscle activation is at 1.0. Active force values from lower levels of activation are also shown to highlight the force-length skew coefficient (dashed line) (adapted from Buchanan et al., 2004).

Passive force arises from muscle fibers stretching beyond their optimal lengths. As seen in Figure 2.5, the passive force is zero before optimal fiber length and increases exponentially thereafter. Schutte (1993) modeled this relationship as

$$\tilde{F}_P = \frac{e^{10(\tilde{l}_m - 1)}}{e^5} \quad (10)$$

where \tilde{l}_m , the normalized muscle fiber length, is determined by dividing muscle length values (solved iteratively by forward integration [Section 2.2.3]) by $l_m^o(t)$. With activation and muscle length values, equations (9) and (10), and the force-length relationship, the active and passive forces in the contractile element of a muscle can be determined.

2.2.2.2 Force-Velocity Relationship

Much of the current knowledge of the force-velocity relationship was founded on A.V. Hill's work (1938). It was observed that muscle force decreases while the muscle is shortening and increases while the muscle is lengthening. The force-velocity relationship is derived at optimal fiber length. Epstein and Herzog (1998) expanded on this and accounted for the force-velocity relationship at other fiber lengths by creating two separate equations for concentric and eccentric contractions,

$$\tilde{F}_{V(\text{concentric})} = \frac{b - a \cdot \tilde{v}_m}{b + \tilde{v}_m} \quad (11)$$

$$\tilde{F}_{V(\text{eccentric})} = F_{ecc} - (F_{ecc} - 1) \frac{b' + a' \cdot \tilde{v}_m}{b' - \tilde{v}_m} \quad (12)$$

The values of a and b , and a' and b' are constants for the concentric and eccentric force equations, respectively. F_{ecc} is the maximum eccentric force multiplier and ranges between 1.1 and 1.8 (Epstein and Herzog, 1998).

The muscle fiber velocity is normalized by the number of optimal fiber lengths per second. This is important to note, because with the use of optimal fiber lengths, the force-velocity relationship is inherently dependent on muscle activation as well from the force-length curve.

2.2.2.3 Damping Component

The final component acting in parallel in the muscle fiber is the damping component, b_m . Schutte et al. (1993) claim this variable is needed to maintain the stability of the muscle. They state that the “addition of this element also diminishes the difficulties associated with inverting the force-velocity relationship when activation is low.” Lloyd and Besier (2003) have used a value of .1 for b_m . To account for this component mathematically, Epstein and Herzog (1998) developed a new equation for velocity dependent force

$$\tilde{F}_V = \frac{\tilde{F}_{vd} - b_m \cdot \tilde{v}_m}{\tilde{F}_A \cdot a(t)} \quad (13)$$

where \tilde{F}_{vd} is the velocity dependent force term directly from the force-velocity curve. The concentric and eccentric force velocity equations (eqs. 11 and 12) are equated to (13) and \tilde{v}_m is initially solved for in both using the quadratic formula (Bassett et al., 2006).

2.2.2.4 Pennation Angle

Because the muscle fiber and tendon act in series, tendon force will equal muscle force. However, the muscle fibers do not typically act in parallel to the tendon. The pennation angle, φ , describes this deviation of the muscle fibers from the tendon through the relationship, $F_t = F_m \cos(\varphi)$. Unfortunately the pennation angle varies with muscle fiber length. Scott and Winter (1991) developed a time dependent equation for the pennation angle,

$$\varphi(t) = \sin^{-1} \left(\frac{l_m^o \cdot \sin(\varphi_o)}{l_m(t)} \right) \quad (14)$$

where φ_o is the pennation angle when the muscle is at optimal fiber length.

2.2.2.5 Tendon Force Relationship

The tendon is an elastic element that helps facilitate movement in bone through muscle forces. Below the tendon slack length, l'_s , the tendon does not produce any

force. Zajac (1989) developed a relationship between the tendon slack length and tendon strain,

$$\varepsilon^t = \frac{l_t - l_s^t}{l_s^t} \quad (15)$$

Once the tendon slack length is reached during contraction, the relationship between force and strain is not simply linear. There is a short nonlinear region as the tendon accepts force where the collagen fibers in the tendon are unloaded. Zajac (1989) described the force-strain relationship as,

$$\tilde{F}_t = 0 \quad \varepsilon \leq 0 \quad (16)$$

$$\tilde{F}_t = 1480.3 \cdot \varepsilon^2 \quad 0 < \varepsilon < 0.0127 \quad (17)$$

$$\tilde{F}_t = 37.5 \cdot \varepsilon - 0.2375 \quad \varepsilon \geq 0.0127 \quad (18)$$

Equation (17) shows the nonlinear region up to a strain of 0.0127 and a linear region thereafter (18). With prior knowledge of tendon length, l^t (i.e. $l_t = l_{mt} - l_m$), only tendon slack length is needed to determine tendon force.

2.2.2.6 Maximum Isometric Force Strength Factors

In order to use normalized values for active, passive, tendon, and velocity dependent force, we need to have a measure of maximum isometric force. As is the

case with all muscle forces, however, measuring true values is challenging because of the indeterminate system. Instead, studies have used anthropometric data to estimate the maximum force (Yamaguchi et al., 1990; Delp et al., 1990). Buchanan (1994) showed that maximum muscle stress is not constant and varies for each subject. To account for this, strength factors are applied to functional muscle groups,

$$F_{\max} = G_f \cdot F_{\max,est} \quad (19)$$

$$F_{\max} = G_e \cdot F_{\max,est} \quad (20)$$

where G_f and G_e are the flexion and extension strength factors and $F_{\max,est}$ is the maximum isometric force data previously reported from literature. Strength factors vary greatly between subjects and are optimized within the EMG-driven model.

2.2.3 Muscle Parameters & Model Optimization

From muscle activation and contraction dynamics, it can be seen that the EMG-driven model requires much information. Musculotendon parameters help define the subject-specific, and in some cases, muscle-specific information. It is important is to know which parameters are specific to each muscle and which can use global parameters applied to all muscles within a certain group. Heine et al. (2003) ran an EMG-driven model varying the number of optimized parameters from 0 to 57.

His results showed that using a 7 parameter model still maintained a reasonably good predictive ability.

The muscle force estimated from an EMG-driven model is dependent on both constant and time-varying variables. Muscle activation dynamics can be used to directly determine the constant, muscle-specific values of γ_1 , γ_2 , d , and A from (1) through (7).

Conversely, muscle contraction dynamics calculates muscle force using a Runge-Kutta-Fehlberg algorithm to numerically integrate the nonlinear differential equation at each time step (Buchanan et al., 2004). Bassett et al. (2006) explains in detail how the relationships described in equations (8) through (20) result in estimated muscle force. Optimized constant, muscle-specific values for F_o^m , l_m^o , l_s^t , and ϕ_o and global values for G_f and G_e are output.

The EMG-driven model attempts to match the forward dynamic joint moment to the inverse dynamic moment by adjusting muscle parameters iteratively. A time efficient simulated annealing algorithm minimizes the difference between the two moments (Goffe et al., 1994). The number of iterations the model is run should be considered because it is important that the model not be calibrated to the extent that it becomes trial specific and lose predictive ability.

The inputs to the model are the EMG, musculotendon lengths, l_{mt} , moments arms, and the inverse dynamic moment. The EMG and musculotendon lengths are all that is needed to carry the model through muscle activation and contraction dynamics

while all other parameters are optimized from initial guesses based on previously reported data. Once the muscle force is determined, the moment arms are used to calculate the total joint moment which is then calibrated to the inverse dynamic moment. Each time a single parameter is adjusted the model is rerun.

2.3 OpenSim Model

OpenSim is an open-source simulation software created for the analysis of the musculoskeletal system. The program allows the user to generate simulations, edit muscle paths and physiology, plot variables of interest, and visualize results. Because the software is available to the public, there is great potential for personal modification and collaborative efforts (Delp et al., 2007). OpenSim offers a unique method to provide computationally efficient forward simulation results based on a computed muscle control algorithm. The steps involved in typical musculoskeletal analysis include model scaling, inverse kinematics, a reduced residual algorithm, and a computed muscle control algorithm. Figure 2.6 shows a schematic of the simulation.

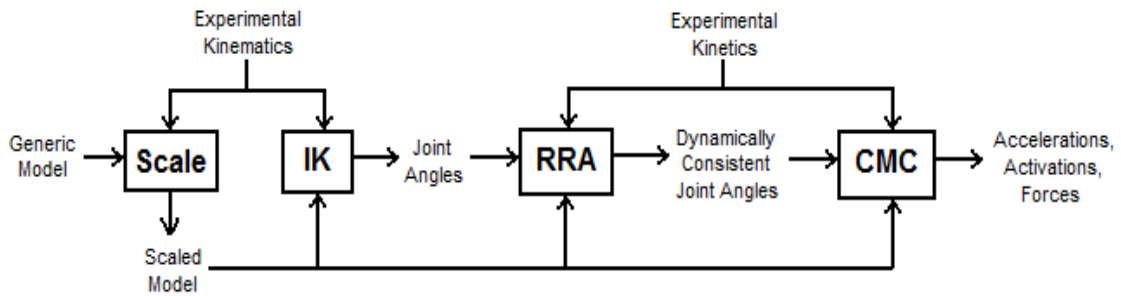


Figure 2.6: OpenSim model schematic showing the steps of musculoskeletal analysis (adapted from Delp et al. 2007).

2.3.1 Model Scaling

OpenSim begins with a generic model that is scaled to match the anthropometry of a particular subject. Distances between pairs of experimental markers are averaged over a static trial and divided by the distance between the identical pair of virtual markers on the generic model to create scale factors. The scale factors are then used to match virtual markers to experimental markers. The segment masses are scaled proportionally to the generic model and the total mass of the subject is preserved (Delp et al., 2007).

2.3.2 Inverse Kinematics

The inverse kinematics solves for a set of generalized coordinates (i.e. joint angles and positions) that best reproduce experimental kinematics. This is determined by the minimization of a weighted least squares equation at each time step,

$$\text{Squared Error} = \sum_{i=1}^{\text{markers}} w_i (x_{i,\text{exp}} - x_i)^2 + \sum_{j=1}^{\text{coordinates}} w_j (q_{j,\text{exp}} - q_j)^2 \quad (21)$$

where $x_{i,\text{exp}}$ and x_i are the experimental and model marker positions, $q_{j,\text{exp}}$ and q_j are the experimental and model coordinates, and w_i and w_j are the weight factors that specify how strongly the error term should be minimized (Delp et al., 2007).

2.3.3 Reduced Residual Algorithm

Reduced residual algorithm (RRA) adjusts the model kinematics to make them more dynamically consistent with experimental data. Because of experimental error, generalized coordinates do not accurately represent measured ground reaction forces leading to dynamic inconsistency. In order to account for Newton's Second Law, a residual force must be added,

$$\vec{F}_{\text{external}} = \sum_{i=1}^{\text{segments}} m_i \vec{a} - \vec{F}_{\text{residual}} \quad (22)$$

The residual forces represent six generalized coordinates (3 residual forces, 3 residual moments) between the model and the ground (Delp et al., 2007). In ideal cases with no experimental error, residual forces will be zero.

The residuals are averaged over the range of motion and optimized using either a slow target (23),

$$J = \sum_{i=1}^{nx} x_i^2 + \sum_{j=1}^{nq} w_j (\ddot{q}_{d,j} - \ddot{q}_j) \quad (23)$$

or fast (24) target cost function,

$$J = \sum_{i=1}^{nx} x_i^2 \quad (24)$$

$$C_j = \ddot{q}_{d,j} - \ddot{q}_j \quad (25)$$

where x_i^2 is the squared actuator controls, $\ddot{q}_{d,j}$ and \ddot{q}_j are the desired and model accelerations, respectively, and w_j is the weighting factor. The first summation in (23) distributes the residual forces across the generalized coordinates while the second summation drives the model accelerations toward the desired accelerations (OpenSim Users Manual).

By comparison, the fast target places a constraint (25) on the accelerations which inherently determines computational speed. The absence of a constraint would let the kinematics be tracked with no problems; however, the resulting residuals would be so large that they will exert forces on the model leading to unrealistic muscle function. Conversely, constraints that are too restrictive will lead to drastic changes in

the kinematics in order to satisfy (24) that likely would not be indicative of true gait. An understanding of the appropriate constraint for a particular task is necessary. After optimization, the dynamically consistent output model is then input into the computed muscle control algorithm.

2.3.4 Computed Muscle Control

Computed muscle control (CMC) determines a set of individual muscle excitations that will drive a musculoskeletal model towards a desired movement. The algorithm is unique because it uses static optimization within a forward dynamic simulation.

In the first stage of CMC, desired accelerations are determined from experimental kinematics and the model kinematics from RRA using a proportional derivative,

$$\ddot{q}_d = \ddot{q}_{\text{exp}} + k_v (\dot{q}_{\text{exp}} - \dot{q}) + k_p (q_{\text{exp}} - q) \quad (26)$$

where \ddot{q}_{exp} , \dot{q}_{exp} , and q_{exp} are the experimental accelerations, velocities, and positions, \dot{q} and q are the model velocities and positions, and k_v and k_p are feedback gains for the velocity and position errors. When the desired accelerations are reached, the model coordinates, q and \dot{q} , will be driven to experimental coordinates, q_{exp} and \dot{q}_{exp} . k_v and

k_p will fall to zero in a critically damped manner by letting $k_v = 2\sqrt{k_p}$ (Thelen et al., 2003) (Figure 2.6).

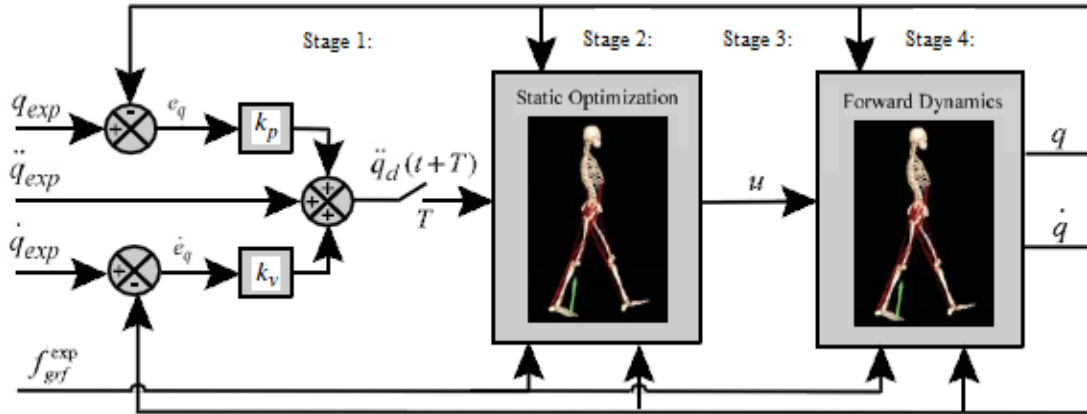


Figure 2.7: Computed muscle control algorithm (Thelen et al., 2003). Desired accelerations, \ddot{q}_d , are determined from experimental position and velocity errors, e_q and \dot{e}_q , and a proportional derivative in stage 1. Steady-state forces are estimated based on a static optimization in stage 2. Muscle excitations that drive these forces are computed in stage 3 are then input into a forward dynamic model that outputs model generalized coordinates.

In the second stage, a static optimization calculates a set of muscle forces that, under steady-state conditions, produce the desired accelerations from the first stage. First, the desired accelerations, along with the equation of motion, outline a redundant system that will be solved for muscle forces. Since there are 58 muscles and only 23 joints, boundary conditions are needed to solve the resulting system of equations. Activation and contraction dynamics are solved using zero and full excitation (i.e. $u =$

0,1) to determine upper and lower bounds for muscle forces at the next time step (Thelen & Anderson, 2006). Once this information is calculated, a cost function, as used in RRA [Equations (23), (24), (25)], is applied to distribute forces across synergistic muscles. Forces are then input into the equations of motion to solve for steady-state accelerations that will assist in determining muscle excitations.

Stage 3 applies a root solver to compute a set of excitations that, when input into the activation and contraction dynamics, would produce the forces determined in stage 2. Excitation values are allowed to range between 0 (no excitation) and 1 (full excitation). The muscle excitations are the only component input into the forward dynamic simulation (Thelen et al., 2003).

The final stage is a forward dynamic model that determines the generalized coordinates using integration to move forward each time step. It is important to note that although a static optimization is used, a full set of time-dependent state equations are used and incorporated in the forward dynamics (Delp et al., 2007; Zajac, 1989),

$$\begin{cases} \dot{a} = \begin{cases} (u - a) / \tau_{act}, & u \geq a, \\ (u - a) / \tau_{deact}, & u < a, \end{cases} \\ \dot{l}_m = f_v^{-1}(l_m, l_{mt}, a) \\ \ddot{q} = A^{-1}(q) \cdot \{G(q) + C(q, \dot{q}) + R(q) \cdot f_m + E(q, \dot{q})\} \end{cases} \quad (28)$$

The output generalized model coordinates are then fed back into stage 1 (26) and the CMC algorithm is repeated again until the entire time range is complete. (Note: In equation 28, \dot{a} = time rate of change of muscle activation; τ_{act} , τ_{deact} = activation and deactivation time constants; f_v = force-velocity relation; A^{-1} = inverse of system mass matrix; G = generalized gravity forces; C = generalized Coriolis and centripetal forces; R = muscle moment arms; f_m = muscle forces; E = generalized external forces).

2.4 Summary

Clinical analysis of the musculoskeletal system can have wide ranging benefits. Knowledge of muscle forces and kinematics can lead to a better understanding of body motion and neural control. Currently, it is challenging to solve for individual muscle forces because of the redundant system, so various methods are used.

Inverse dynamics uses kinematic data and ground reaction forces to calculate joint moments. A static optimization is then solved distributing loads appropriately across synergistic muscles.

Conversely, forward dynamics uses muscle excitations or joint kinetics along with a full set of state equations to calculate joint kinematics and iteratively drive the model forward. While this method is much more time intensive than static optimization, forward dynamics is a better representation of actual neuromuscular physiology because it accounts for the duration of a movement as opposed to single instances in time.

Finally, EMG-to-force models also perform an optimization, but with the advantage of insight into actual muscle activity. A cost function minimizes the difference between joint moments by iteratively altering muscle parameters resulting in subject-specific values. Once the cost function is satisfied and optimized parameters are attained, activation and contract dynamics calculates the estimated individual muscle forces.

Musculoskeletal parameters such as tendon slack length, optimal fiber length, and maximum isometric force are critical to the clinical relevance of these models. Inaccurate parameter estimates will greatly hinder their predictive ability. Using published results of muscle parameters from cadavers is the standard procedure in forward dynamic simulations (Delp et al., 1990; Yamaguchi et al., 1990). Although these are sufficient approximations, there is an inherent limitation because they cannot account for differences in muscle physiology from a wide range of subjects. The intent of this study is to determine how optimized, subject-specific parameters from an EMG-driven model, as opposed to generic parameters, will affect the accuracy of an OpenSim forward dynamic simulation.

EMG-driven models have also been able to model stroke patients (Shao et al., 2009). It is our belief that in future studies, forward dynamic simulations using subject-specific parameters from individuals with pathological gait can give insight into neuromuscular deficiencies that can help tailor rehabilitation programs.

Chapter 3

METHODS

3.1 Experimental Data

3.1.1 Walking Trials

Three-dimensional kinematic and kinetic data were collected from 3 healthy subjects (24 ± 1 year, 86.4 ± 8.2 kg, 179.5 ± 12.0 cm) walking on a split-belt, motorized treadmill (Bertec Corp., Columbus, OH) at their self-selected speed. Healthy subjects, those with no previous heart condition or lower limb injury, signed informed consent forms approved by the human subject review board of the University of Delaware. An 8-camera Motion Analysis system (Santa Rosa, CA) was used to record the three-dimensional locations of 27 markers in static trials and 23 markers in dynamic trials at 60 Hz. Static trials lasted 5 seconds and included medial knee and ankle markers used to determine joint centers. Dynamic trials were run for 30 seconds and ground reaction force data was collected from 2 symmetric forceplates at 1080 Hz.

3.1.2 Electromyography Data

Electromyography (EMG) data were collected at 1000 Hz for maximum voluntary contraction trials and 1080 Hz for waking trials from surface electrodes (Motion Laboratory Systems, Baton Rouge, LA) on 9 major knee and ankle muscles of

a lower limb: rectus femoris (RF), vastus medialis (VM), vastus lateralis (VL), biceps femoris long head (BFLH), semitendinosus (ST), medial gastrocnemius (MG), lateral gastrocnemius (LG), soleus (Sol), and tibialis anterior (TA). The lower limb was wrapped to minimize noise and electrode placement was maintained between walking and maximum voluntary contraction trials.

3.1.3 Maximum Voluntary Contraction Trials

Maximum voluntary contraction (MVC) trials were collected using a Biodex System 3 Pro dynamometer (Biodex, Shirley, NY, USA). To account for variability in muscle activity between tasks, both isometric and isokinetic trials were collected. Isometric knee flexion and extension was performed at 90° and isokinetic knee flexion and extension was collected with starting positions of full extension and 90° flexion, respectively. Ankle MVC trials were performed starting in both full dorsiflexion and plantar flexion.

3.1.4 Data Preprocessing

The raw EMG from the walking trials were first high-pass filtered using a forward and reverse pass fourth order Butterworth filter with a cutoff frequency of 50 Hz, then rectified by taking the absolute value of the data. After a low-pass filter with a 4 Hz cutoff frequency was applied, the EMG was normalized to peak values of the

rectified, low-pass filtered MVC data. A single peak value was determined for each muscle from all 16 isometric and isokinetic trials together.

Kinematic and kinetic data acquired from the split-belt treadmill were preprocessed in Cortex 1.0.0.198 (Motion Analysis Corp., Santa Rosa, CA). Matlab (MathWorks Inc., Natick, MA) was used to transform experimental data into the appropriate coordinate system to allow compatibility with OpenSim.

3.2 The EMG-driven Model

The EMG-driven model estimated individual muscle forces by iteratively altering musculoskeletal parameters, attempting to minimize the difference between the forward and inverse dynamic joint moments (Buchanan et al., 2004). The resulting optimized parameters are said to be subject-specific and therefore provide predictive ability of muscle forces for novel tasks. A detailed methodology of the EMG-driven model was explained in Section 2.2. Here, we describe the structure of the model and the data inputs.

3.2.1 Model Structure

The EMG-driven model is a single joint model, meaning only the data and parameters from muscles of a particular joint are included in the optimization. Muscles spanning two joints (i.e. gastrocnemius) are considered independently. Simulated annealing (Goffe et al., 1994) was used to calibrate the forward and inverse

dynamic joint moments and optimize 3 global (λ , G_f , G_e) and 6 muscle-specific (γ_1 , γ_2 , d , A , l_m^o , l_s^i) parameters. The model was run for both the ankle and knee joints of the lower limb.

The ankle joint model included 4 muscles: MG, LG, TA, and Sol. In order to account for all major muscles of the knee, we needed to estimate EMG values for the underlying muscles vastus intermedius (VI), biceps femoris short head (BFSH), and semimembranosus (SM) where surface electrodes were not possible. Because of similar function and insertion points, EMG values for BFLH and ST were used for BFSH and SM, respectively. VI was determined by averaging VM and VL. In total, the knee joint included 10 muscles: RF, VM, VI, VL, BFLH, BFSH, SM, ST, MG, and LG.

3.2.2 Model Inputs

First, the filtered, rectified, and normalized EMG were input into the model. From the entire walking trial, only the section of interest (stance phase, in this case), along with a data padding region, was removed from the EMG data. The data padding region acts as a buffer at the beginning of the stance phase to account for the electromechanical delay of each muscle and included ten additional kinematic data points. The model does not include this region when calibrating the forward and inverse dynamic joint moment.

The normalized force-velocity and active and passive force-length curves were input to help determine optimal muscle fiber lengths and velocities for each muscle (Figure 2.5). The normalized tendon force-strain relationship was also input to describe the initial nonlinear loading region and subsequent linear region.

Musculoskeletal parameters that were optimized in the EMG-driven model were given initial values and constrained within a physiologically relevant range. To maintain consistency within the models, the initial values of maximum isometric force, optimal fiber length, and tendon slack length from OpenSim scaling were used (Section 3.3; Table 3.2). The physiological ranges used to optimize the parameters were based on previous literature (Table 3.1). The global force-length skew coefficient was allowed to move between zero and 0.25 although it has been shown to consistently optimize to approximately 0.15 (Lloyd & Besier, 2003). The pennation angle at optimal fiber length, φ_o , is a muscle-specific parameter, but was not optimized because it has been shown that values are consistent across individuals (Yamaguchi et al., 1990).

Table 3.1: The physiological ranges between which the global and muscle-specific parameters can be optimized. Strength factors, G_f and G_e , apply across functional groups of muscles.

Parameter	Lower Boundary	Upper Boundary	Reference
F-L Skew Coefficient, λ	0	0.25	Lloyd & Besier, 2003
Strength Factors, G_f, G_e	0.5	2.0	Buchanan, 1994; Lloyd & Besier, 2003
Filter Coefficients, γ_1, γ_2	-0.9	0.9	Bassett et al., 2006
Electromechanical Delay, d	0	100 msec	Corcos et al., 1992
Shape Factor, A	0.01	0.12	Manal & Buchanan, 2003
Optimal Fiber Length	OFL · .95	OFL · 1.05	Lloyd & Buchanan, 1996; Xiao et al., In Press.
Tendon Slack Length	TSL · .85	TSL · 1.15	Delp et al., 1990

Muscle moment arms, musculotendon lengths, and the inverse dynamic joint moment are also needed as inputs. Inverse kinematics in OpenSim was run for the desired time range and the necessary moment arms and musculotendon lengths were exported. Finally, the segment masses and joint angles from inverse kinematics (IK) were used to determine the joint moments from inverse dynamics.

3.3 OpenSim Simulation

A three-dimensional model enabling movement in the sagittal, frontal, and coronal planes was built in OpenSim with 13 segments and 23 degrees of freedom (DOF). The head, arm, and trunk (HAT) was modeled as a rigid segment with three rotational DOFs about the pelvis. The hip joint had 3 DOFs and both the knee and

ankle joint had one rotational DOF. The metatarsophalangeal and ankle subtalar joint were weighted to fix the movement and simplify the model.

3.3.1 Model Compatibility

The generic OpenSim model consists of 54 muscles. To maintain consistency between both models, the muscles used for the knee and ankle joints in OpenSim matched the muscles used in the EMG-driven model. OpenSim was not permitted to distribute forces to muscles that were not included in the optimization of the EMG-driven model. In each limb, 3 muscles were removed (sartorius, gracilis, tibialis posterior) and 5 were added (SM, ST, LG, VM, VL) for a net gain of 2 muscles. The adjusted model was actuated by 58 muscles.

3.3.2 Scaling, Inverse Kinematics, & Inverse Dynamics

Scaling, inverse kinematics, and inverse dynamics were all performed before the EMG-model was run so that necessary inputs could be obtained. Scale factors were created to match virtual markers on the generic model to experimental markers. Based on subject height and weight, segment masses were scaled proportionally and total mass was preserved. Table 3.2 shows initial values for the generic model before scaling in OpenSim.

Table 3.2: OpenSim generic model initial values.

Muscle	Maximum Isometric Force (N)	Optimal Fiber Length (m)	Tendon Slack Length (m)
RF	1169	0.114	0.310
VM	1294	0.089	0.126
VI	1365	0.087	0.136
VL	1871	0.084	0.157
BFLH	896	0.109	0.326
BFSH	804	0.173	0.089
SM	1288	0.080	0.359
ST	410	0.201	0.256
MG	1558	0.060	0.390
LG	683	0.064	0.380
Sol	3549	0.050	0.250
TA	905	0.098	0.223

Scaling and IK both used weight factors to describe how strongly the marker positions were tracked. For scaling, weight factors are not critical, however, during IK, appropriate values are necessary to accurately simulate experimental gait (Section 2.3). Table 3.3 shows the values used for both functions. Medial knee and ankle markers were used in static trials to determine joint centers and then removed for dynamic trials.

Lastly inverse dynamics was used to estimate joint torques. OpenSim uses a least squares approach by taking the generalized coordinates obtained in IK and relates two sets of equations that treat all segments simultaneously and solves for joint torques. The system is overdetermined and a static optimization is created to minimize the difference between the torque measurements (Kuo, 1998).

Table 3.3: Weight factors for scaling and IK.

Marker Position	Scaling	Inverse Kinematics
L,R Thigh	1	1
L,R Shank	1	1
Sternum	10	100
Offset	10	100
L,R Shoulder	900	100
V. Sacral	1000	1000
L,R ASIS	1000	1000
L,R Knee	1000	1000
L,R Knee Medial	1000	N/A
L,R Ankle	1000	1000
L,R Ankle Medial	1000	N/A
L,R Heel	1000	500
L,R Toe	1000	500

3.3.3 Reduced Residual Algorithm & Computed Muscle Control

Two fundamental OpenSim models were created for simulation: generically scaled (scaled) and EMG-driven model optimized (optimized). The scaled model simply used the parameter values based on the weight factors. The optimized model used subject-specific parameters determined within the EMG-driven model. After the EMG-driven model was run, the generically scaled OpenSim musculoskeletal parameters were replaced with subject-specific parameters. Optimized values of maximum isometric force, optimal fiber length, and tendon slack length were applied across 12 knee and ankle muscles for a total of 36 subject-specific parameters for each lower limb. Since we used healthy subjects, symmetry was assumed and parameters were consistent across both limbs. Because the gastrocnemius is a biarticular muscle,

strength factors from the knee flexors and ankle plantar flexors were averaged and applied to generic maximum isometric force values. Similarly, optimized values of optimal fiber length and tendon slack length from the EMG-driven model were averaged for LG and MG.

The reduced residual algorithm tool adjusted the model kinematics to be more dynamically consistent with experimental data. Residuals were applied to account for experimental error and satisfy Newton's Second Law. A computed muscle control (CMC) algorithm was then used to estimate generalized coordinates (joint positions and velocities) by incorporating a static optimization within a forward simulation which drastically reduced computational time (Section 2.3). CMC provides an efficient way to solve a redundant system and distribute forces across muscles. Individual muscle forces and activations were used as a means to compare the EMG-driven model and OpenSim.

3.4 Model Comparison & Calculations

In calibrating the EMG-driven model to a particular subject's walking trial, the forward dynamic joint moment attempted to match the input inverse dynamic moment. Coefficient of determination (r^2), root mean square (RMS) error, and root mean square error normalized to peak-to-peak values were calculated for both knee and ankle joints. The knee and ankle joint models both separately estimated muscle activations and forces for the biarticular gastrocnemius. Peak values and corresponding percent

differences were reported to show the model's variability. Though each model produces these values independently, averages from the two (MG, LG) are used for all subsequent model comparisons.

Muscle activation and force were compared to observe differences between the EMG-driven model and the optimized and generically scaled OpenSim models. The trapezoidal rule was used to determine the total area under each curve for all 12 muscles. First, a ratio of the areas of the two OpenSim models was determined (scaled/optimized). Then, ratios were calculated comparing the EMG-driven model to both OpenSim models (EMG-driven/scaled; EMG-driven/optimized).

Finally, the EMG-driven model and OpenSim outputs were compared to see how well net forces matched even with different optimization cost functions. Net knee forces were determined by calculating the difference between flexors (BFLH, BFSH, SM, ST, MG, LG) and extensors (RF, VM, VI, VL) while net ankle forces were the difference between plantar flexors (MG, LG, Sol) and dorsiflexors (TA). To quantify the overall comparison from net muscle forces, r^2 , RMS, normalized RMS, and peak force differences were calculated. Scaled and optimized OpenSim models were compared to the EMG-driven model, as well as to each other.

Chapter 4

RESULTS

4.1 EMG-driven Model

4.1.1 Model Calibration

The forward dynamic moment from the EMG-driven model matched the input inverse dynamic moment with relatively good accuracy. The model was calibrated to the ankle and knee moments (Fig. 4.1). The average r^2 value across all subjects and joints was approximately 0.94 (Table 4.1). The r^2 values ranged from 0.842 to 0.968 and normalized RMS error was between 0.053 and 0.097. Individual muscle activations and forces output from the EMG-driven model were compared to OpenSim forward simulation results.

Table 4.1: Individual and averaged r^2 , RMS, and normalized peak-to-peak RMS error values for the EMG-driven forward dynamic calibration of joint moments.

	r^2	RMS (Nm)	Normalized RMS
Subject 1			
Ankle	0.965	8.86	0.056
Knee	0.968	4.92	0.053
Subject 2			
Ankle	0.944	13.04	0.075
Knee	0.842	13.82	0.097
Subject 3			
Ankle	0.953	11.14	0.072
Knee	0.962	4.53	0.058
AVERAGE			
Ankle	0.954	11.01	0.068
Knee	0.924	7.76	0.069

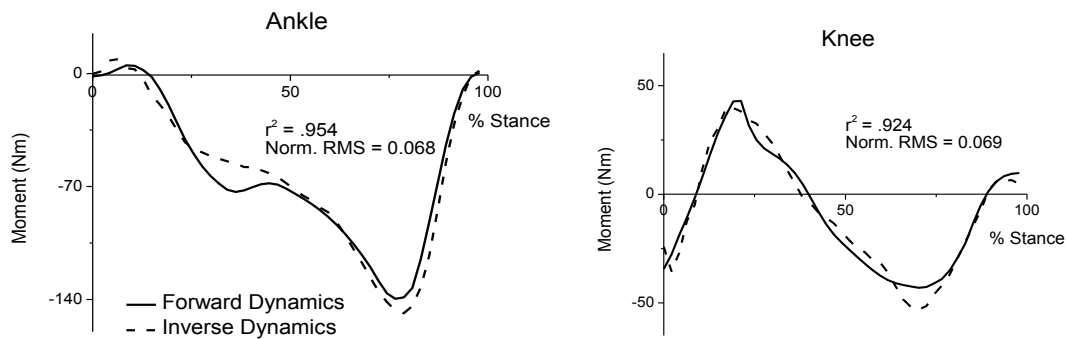


Figure 4.1: Average calibrated forward dynamics moment from the EMG-driven model. The forward dynamic (bold line) moment matched the inverse dynamic (dashed line) moment input for the ankle and knee.

4.1.2 Optimized Parameters

Generic values of the optimal fiber length (OFL), and tendon slack length (TSL) from OpenSim were scaled to subject dimensions and used as initial values in the EMG-driven model. Percent differences in OFL from generic to optimized values varied from -4.96 to 5.0 across subjects, however most showed an increase in length from scaled to optimized values, with the exception of LG and Sol (Table 4.2). Also, the majority of muscles did not reach the constraint of $\pm 5\%$ for OFL and had similar optimized and generically scaled values. Percent differences in TSL varied from -14.70 to 8.76 (Table 4.2). Contrary to OFL where an increase in length was seen, most TSL's were shortened from scaled values. In general, the vasti muscles had largest decreases in TSL. Conversely, Sol, SM, and the biceps femoris showed the smallest percent differences.

Table 4.2: Average (OpenSim) scaled and (EMG-driven model) optimized values for all subjects with percent differences for optimal fiber length and tendon slack length. Scaled and optimized ratios of tendon slack length to optimal fiber length are shown in the far right columns.

Muscle	Optimal Fiber Length			Tendon Slack Length			l'_s/l'_m	
	Scaled	Opt.	% Diff.	Scaled	Opt.	% Diff.	Scaled	Opt.
RF	0.109	0.109	0.74	0.296	0.292	-1.61	2.72	2.68
VM	0.084	0.085	0.37	0.119	0.104	-12.61	1.42	1.22
VI	0.082	0.084	2.19	0.128	0.114	-10.58	1.56	1.36
VL	0.080	0.080	0.53	0.149	0.136	-9.05	1.86	1.70
BFLH	0.077	0.079	2.94	0.385	0.372	-3.72	5.00	4.71
BFSH	0.101	0.102	1.94	0.305	0.294	-5.15	3.02	2.88
SM	0.061	0.064	4.92	0.294	0.285	-2.33	4.82	4.45
ST	0.132	0.134	2.66	0.238	0.224	-5.52	1.80	1.67
MG	0.072	0.075	3.63	0.364	0.339	-7.24	5.06	4.52
LG	0.154	0.150	-0.87	0.296	0.287	-3.57	1.92	1.91
Sol	0.088	0.086	-1.21	0.297	0.293	-0.68	3.38	3.41
TA	0.147	0.149	1.73	0.132	0.123	-7.70	0.90	0.83

Initial values for maximum isometric force (MF) in the EMG-driven model were also taken from OpenSim. However, unlike TSL and OFL, generic values of MF are not scaled to subject dimensions. In the EMG-driven model, changes in MF were accounted for by strength factors ranging from 0.5 to 2.0 applied across the functionally similar muscle groups of knee flexors and extensors and ankle dorsiflexors and plantar flexors ($MF_{optimized} = G_{f,e,df,pf} \cdot MF_{generic}$). Subject 1 had ankle strength factors that reached 2.0 and knee strength factors just below their level of constraint (Table 4.3). Subject 2 also had strength factors close to saturation, while subject 3 was in the middle of the physiological range. The corresponding MF values

were averaged for all subjects and shown in comparison to initial generic values (Table 4.3).

Table 4.3: Generic (OpenSim) and averaged optimized maximum isometric force values from all subjects based on strength factors from the EMG-driven model.

			Maximum Isometric Force				
			Generic	Optimized			
			Muscle	Average	S.D.		
Knee	Average	S.D.	RF	1169	2311	36	
	G_e :	1.977	0.031	VM	1294	2558	40
	G_f :	1.705	0.507	VI	1365	2698	42
				VL	1871	3698	58
Ankle	Average	S.D.	BFLH	896	1527	455	
	G_{df} :	1.954	0.080	BFSH	804	1371	408
	G_{pf} :	1.805	0.243	SM	1288	2196	654
				ST	410	699	208
				MG	1558	2734	388
				LG	683	1198	170
				Sol	3549	6404	864
				TA	905	1768	72

4.1.3 Activation and Force for the Biarticular Gastrocnemius

The EMG-driven models for the knee and ankle produced varying peak activations and forces in the MG and LG. Percent differences in peak values ranged from -37.9 to -1.6 for activations and -53.5 to 59.3 for forces (Table 4.4). Knee and ankle model values were averaged and used for comparison to OpenSim values in the subsequent sections.

Table 4.4: Peak values and percent differences of the MG, LG forces and activations from the knee and ankle EMG-driven models.

	ACTIVATIONS			FORCES		
	Knee	Ankle	% Diff.	Knee	Ankle	% Diff.
Subject 1						
MG	0.557	0.481	-13.6	1756	1152	-34.4
LG	0.393	0.244	-37.9	576	268	-53.5
Subject 2						
MG	0.424	0.416	-1.9	854	1360	59.3
LG	0.258	0.254	-1.6	186	265	42.5
Subject 3						
MG	0.553	0.522	-5.6	1798	986	-45.2
LG	0.368	0.285	-22.6	515	245	-52.4
AVERAGE						
MG	0.511	0.473	-7.046	1469	1166	-6.8
LG	0.340	0.261	-20.673	426	259	-21.1

4.2 Muscle Activation & Force Comparison for OpenSim & EMG-driven Models

4.2.1 Knee Extensors

Average muscle activations using generically scaled OpenSim parameters were higher than activations using optimized parameters for all knee extensors (Table 4.5, scaled/optimized; Figure 4.2). Optimized activations were more similar to the EMG-driven model in magnitude and timing of peaks with ratios closer to 1.0 (Table 4.5, EMG-driven/scaled, EMG-driven/optimized). The range of activation ratios of EMG-driven/optimized was 0.533 to 1.217. Peak values for all muscles occurred between 20 and 50% of stance phase. While scaled and optimized activations showed greater

point-to-point variability throughout stance, EMG-driven model values consistently remained below .25.

Table 4.5: Muscle activation ratios using average area under curve from the Trapezoidal Rule.

Muscle	Scaled/Optimized	EMG-driven/Scaled	EMG-driven/Optimized
RF	1.045	0.521	0.533
VM	1.735	0.539	0.917
VI	1.838	0.625	1.150
VL	1.850	0.628	1.217
BFLH	3.244	0.308	0.907
BFSH	0.969	0.174	0.157
SM	2.899	0.201	0.491
ST	3.293	0.334	0.750
MG	1.361	0.513	0.700
LG	2.070	0.478	1.014
Sol	1.690	0.956	1.526
TA	1.399	0.679	0.946

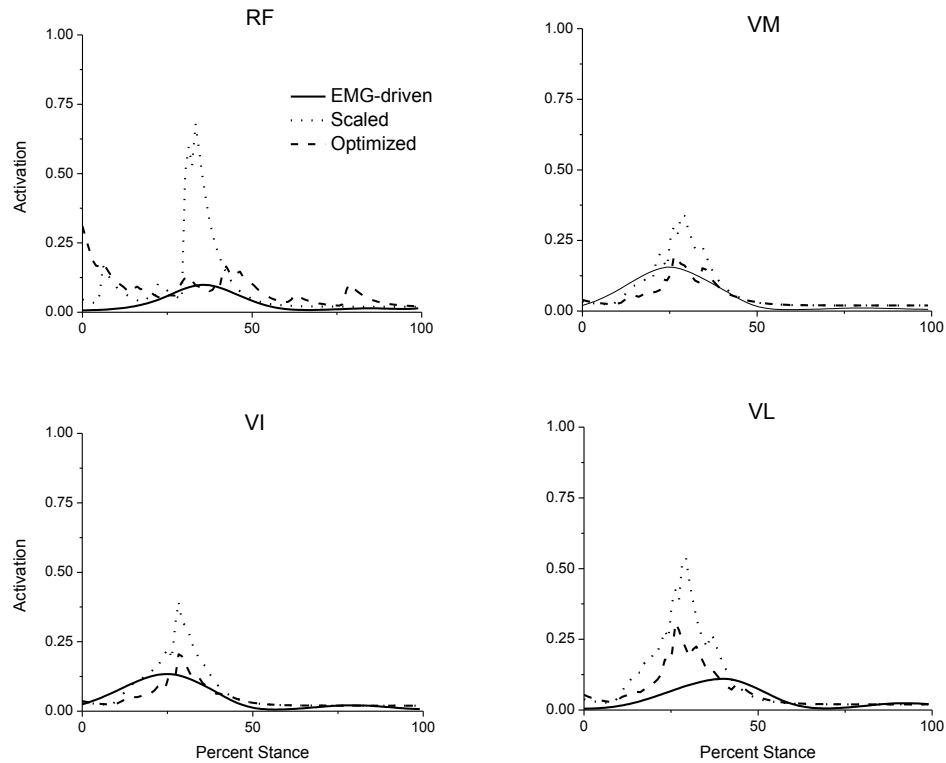


Figure 4.2: Muscle activations of the knee extensors for subject 1.

Contrary to activations, individual knee extensor muscle forces using scaled parameters were lower than forces using optimized parameters (Table 4.6; Figure 4.3). All scaled/optimized ratios were below 1.0 and ranged from 0.644 to 0.892. EMG-driven model forces varied across subjects showing magnitudes both above and below scaled and optimized values. Optimized and EMG-driven model peak forces reached approximately 800N even though the force generating capability is as high as 3600N in some muscles.

Table 4.6: Muscle force ratios using average area under curve from the Trapezoidal Rule.

Muscle	Scaled/Optimized	EMG-driven/Scaled	EMG-driven/Optimized
RF	0.892	0.914	0.733
VM	0.644	1.148	0.731
VI	0.655	1.264	0.831
VL	0.711	1.272	0.920
BFLH	0.959	0.694	0.628
BFSH	0.637	0.274	0.160
SM	0.665	1.487	0.696
ST	0.910	0.540	0.410
MG	0.765	1.013	0.775
LG	0.849	1.009	0.859
Sol	1.145	1.191	1.362
TA	0.678	1.099	0.747

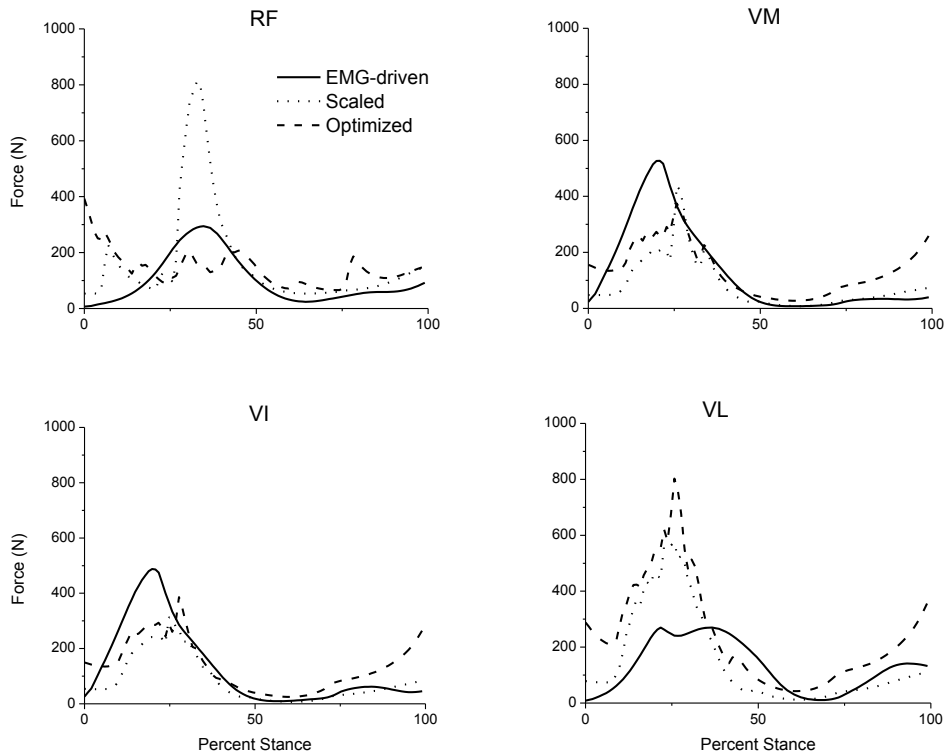


Figure 4.3: Muscle forces of the knee extensors for subject 1.

4.2.2 Knee Flexors

Average optimized knee flexor activations were lower than generically scaled activations for all muscles except BFSH with scaled/optimized activation ratios ranging from 0.969 to 3.293 (Table 4.5; Figure 4.4). Similarly, optimized activations matched EMG-driven activations more closely in all muscles except BFSH with EMG-driven/optimized ratios closer to 1.0. Peak activation values across models occurred in the first 15% of stance. BFSH, SM, and ST showed a second peak for the scaled and optimized activations in late stance that were not seen in EMG-driven

activations. Knee flexors, similar to knee extensors, had EMG-driven activations all below 25% of full activation.

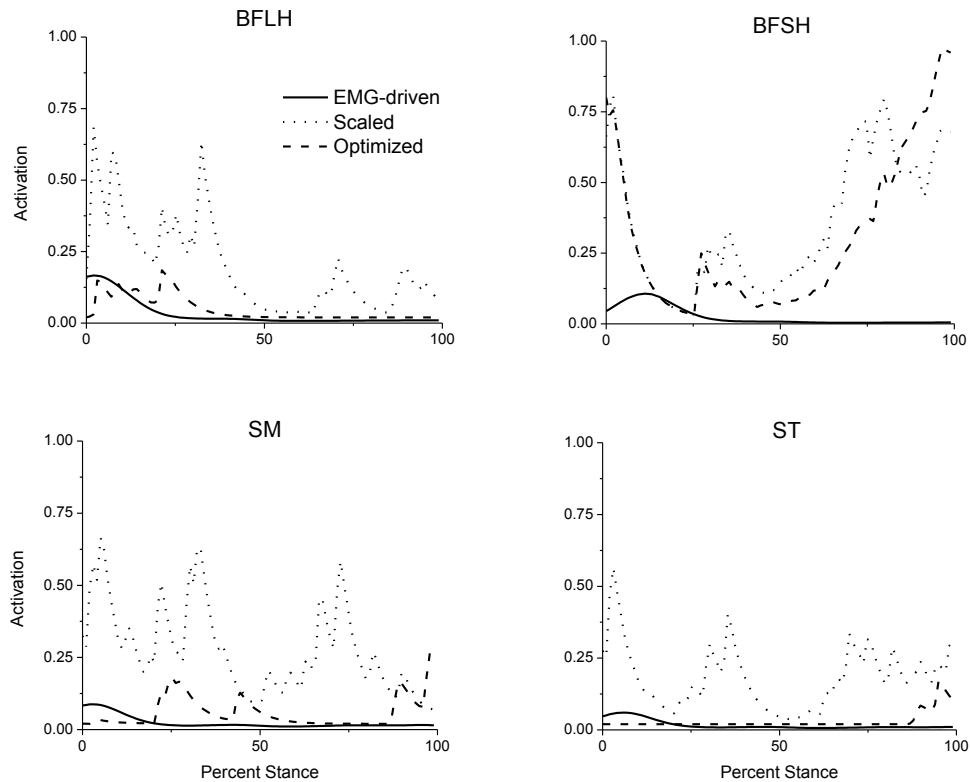


Figure 4.4: Muscle activations of the knee flexors for subject 1.

Knee flexor muscle force varied greatly among the models. Using optimized parameters, OpenSim tended to output forces in the same general shape as EMG-driven forces. However, the second peaks seen in muscle activation for the BFSH, SM, and ST led to similar peaks in force values in late stance (Table 4.6; Figure 4.5). Knee flexor forces for all subjects were low throughout stance, with peak values

ranging from 13.3 to 91.5% of their force generating ability, matching similar low activation levels. Initial peak forces occurred within the first 15% of stance for all muscles.

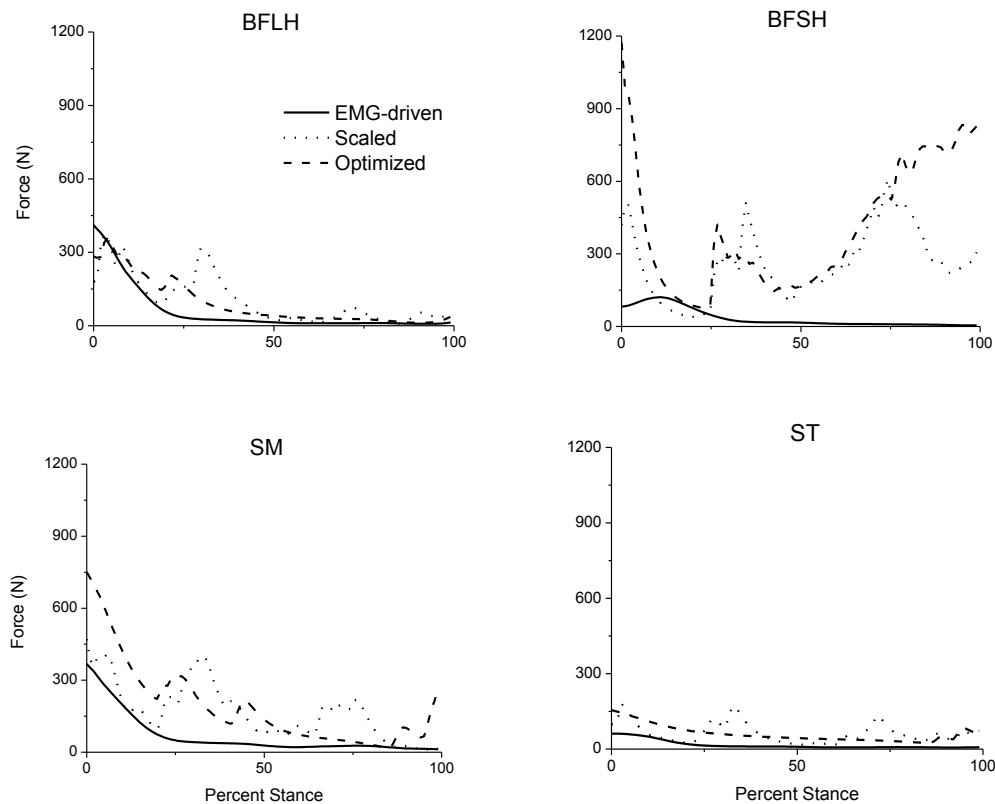


Figure 4.5: Muscle forces of the knee flexors for subject 1.

4.2.3 Ankle Plantar Flexors & Dorsiflexors

Activation of ankle muscles was greater than both knee flexors and extensors. The scaled OpenSim model showed the largest activations across all muscles, at times reaching levels of full activation (Table 4.5; Figure 4.6). All muscles had scaled/optimized activation ratios above 1.0 ranging from 1.361 to 2.070. Using

optimized parameters lowered average activation levels closer to EMG-driven values in all muscles except the Sol (Table 4.5). The plantar flexors (MG, LG, Sol) were consistent in timing and pattern showing peak values at approximately 75% of stance. TA also showed similarity in timing, with peak activations occurring within the first 25% of stance when the muscle controls the foot movement from heel-strike to foot-flat.

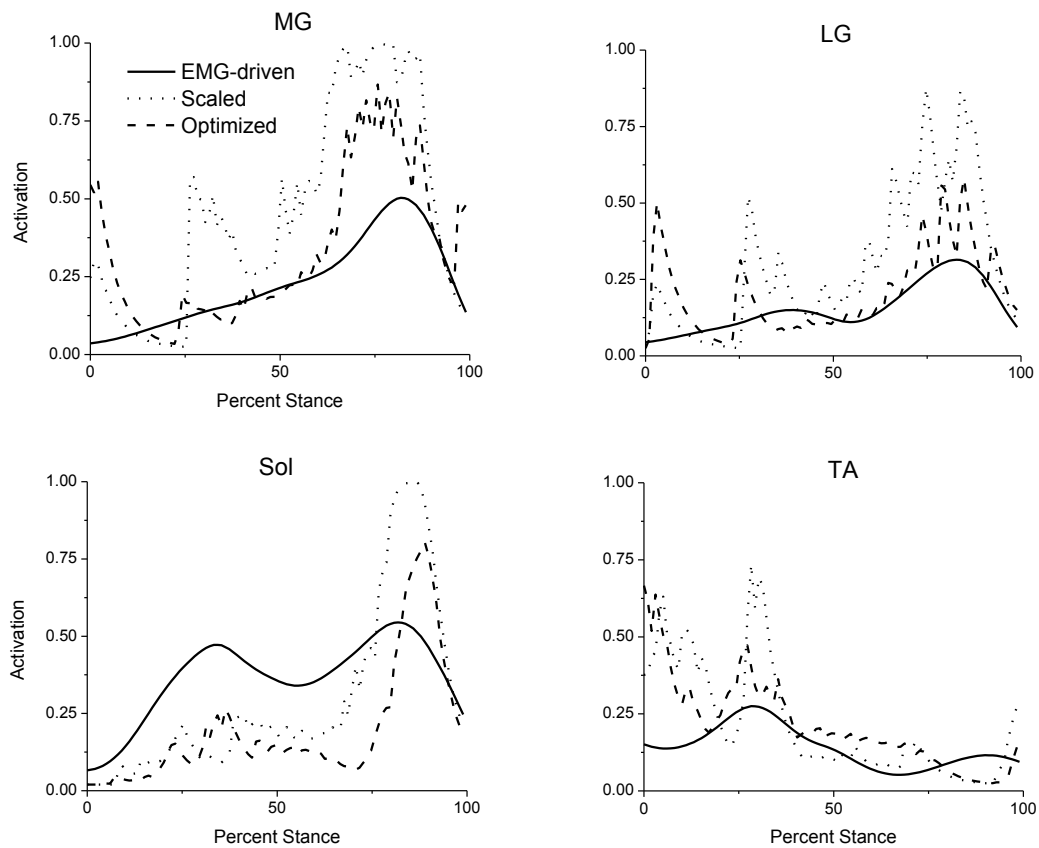


Figure 4.6: Activations of the ankle muscles for subject 1. Knee and ankle EMG-driven model activations of the biarticular MG and LG were averaged throughout stance.

Although activations were lower using optimized parameters, average muscle forces were greater than forces using scaled parameters except for the Sol muscle. Scaled/optimized ratios ranged from 0.678 to 1.145 (Table 4.6). OpenSim scaled and optimized forces varied in relation to EMG-driven forces. Optimized muscle forces showed higher peak values for MG and lower peak values for Sol (Figure 4.7). Although optimized activation levels for MG were lower than scaled values, MG force was greater because of a larger force generating ability. Timing and pattern of force values for all muscles were similar, consistent with activation levels.

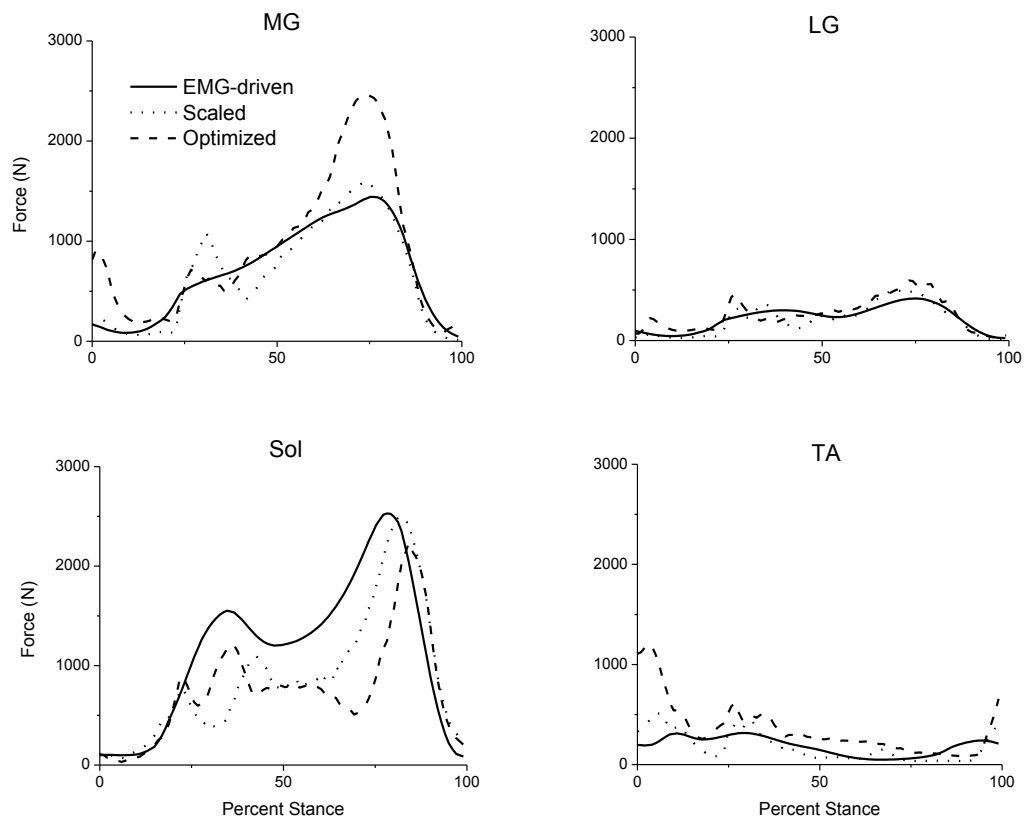


Figure 4.7: Forces of the ankle muscles for subject 1.

4.2.4 Net Joint Forces

While large variability was seen in individual muscle forces, net forces were used to make a global comparison of joint forces. Net ankle forces showed great similarity in pattern, timing, and magnitude between the EMG-driven and OpenSim models with r^2 values ranging from 0.917 to 0.999 (Table 4.7; Figure 4.8). Differences as large as 1600N were seen in the peak values of net knee forces (Table 4.7, diff. in peak), but maintained similar shape and timing. Similar to patterns seen in Figure 4.8, r^2 values were higher for the ankle than the knee where r^2 values ranged from 0.737 to 0.989. Consistent with r^2 values, normalized RMS error was less in the ankle. Differences in peak forces varied across subjects, but were still larger for the knee joint.

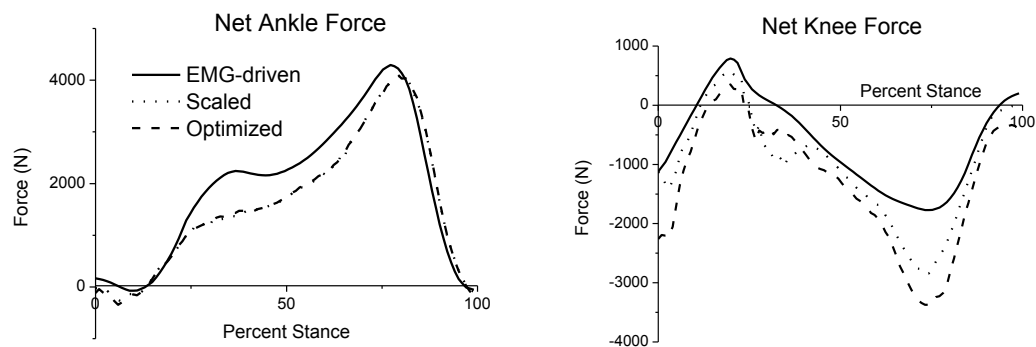


Figure 4.8: Net knee and ankle joint forces for subject 1. Net knee force was calculated as the difference between extensors and flexors and net ankle force was the difference between plantar flexors and dorsiflexors.

Table 4.7: r^2 , RMS, and normalized peak-to-peak RMS error values for the net knee and ankle force for all subjects. Comparisons were made between both the scaled and optimized OpenSim model and the EMG-driven model. Additionally, a comparison between the scaled and optimized models was performed.

ANKLE	r^2	RMS (N)	Normalized RMS	Diff. in Peak (N)
Subject 1				
Scaled/Optimized	0.999	38	0.009	24
EMG-driven/Scaled	0.925	477	0.104	214
EMG-driven/Optimized	0.929	469	0.101	190
Subject 2				
Scaled/Optimized	0.999	48	0.012	24
EMG-driven/Scaled	0.956	305	0.071	592
EMG-driven/Optimized	0.959	299	0.070	568
Subject 3				
Scaled/Optimized	0.998	57	0.014	12
EMG-driven/Scaled	0.917	529	0.119	414
EMG-driven/Optimized	0.914	536	0.120	426
KNEE	r^2	RMS (N)	Normalized RMS	Diff. in Peak (N)
Subject 1				
Scaled/Optimized	0.936	402	0.101	527
EMG-driven/Scaled	0.913	491	0.135	1072
EMG-driven/Optimized	0.919	778	0.187	1600
Subject 2				
Scaled/Optimized	0.989	167	0.054	129
EMG-driven/Scaled	0.751	487	0.151	534
EMG-driven/Optimized	0.737	589	0.173	663
Subject 3				
Scaled/Optimized	0.848	481	0.152	495
EMG-driven/Scaled	0.740	437	0.146	156
EMG-driven/Optimized	0.907	391	0.116	651

Chapter 5

DISCUSSION

In this study, we compared the functionality of two computer based musculoskeletal models using both generic and subject-specific muscle parameters. Specifically, we used optimized values of maximum isometric force, optimal fiber length, and tendon slack length to compare differences in force and activation in knee and ankle joint muscles using a walking trial. Results showed that an OpenSim model using subject-specific parameters, as opposed to generic parameters, produced muscle activation patterns more similar to the EMG-driven model for all muscles except BFSH and Sol.

Comparison of optimized OpenSim and EMG-driven models revealed that, although the models incorporated similar muscle physiology, muscle forces varied throughout the knee and ankle. The models, however, produced encouraging results such that r^2 values for net ankle joint forces were above 0.90 across all subjects. The fact that net joint forces were matched well despite variation within individual muscle forces shows that the difference in cost functions is a significant factor to model outputs. This chapter discusses the differences in the musculoskeletal models and the benefits of using subject-specific muscle parameters.

5.1 Determination of Optimized Muscle Parameters

The basis for this study was the belief that the use of subject-specific muscle parameters can improve gait simulations in OpenSim by producing forces and activations that more closely resemble in vivo values. Currently, generic parameters based on cadaveric studies are scaled to match subject height and weight. While these estimates can provide reasonable results (Anderson & Pandy, 2001a; Anderson & Pandy, 2001b; Neptune et al. 1998; Neptune et al., 2001), it is well known that muscle physiology varies significantly between individuals (Lieber, 1993; Fukunaga et al., 1997; Zajac et al., 2002; Thelen, 2003; Narici et al., 2008).

Several studies have used medical imaging to determine muscular physiology (Arnold et al., 2000; Rugg et al., 1990; Mungiole and Martin, 1990). These can be expensive and are not typically feasible. Others have used EMG-to-force approaches and optimization techniques (Garner & Pandy, 2003; Buchanan et al., 2004). Our study incorporated an EMG-driven model that applied a simulated annealing algorithm that iteratively estimated muscle parameters based on a particular subject's experimental data. We chose to use optimized values of maximum isometric force (MF), optimal fiber length (OFL), and tendon slack length within OpenSim because these parameters have shown to have the most influence on simulation results (Delp & Zajac, 1992; Out et al., 1996; Heine et al., 2003; Scovil & Ronsky, 2006; Redl et al., 2007).

Muscle parameters were held within physiological constraints to maintain relevance within the structure of the body. Scovil and Ronsky (2006) used a perturbation size of 50% that was found to be too large to reproduce kinematic data. Conversely, Redl et al. (2007) used perturbation sizes of 2.5%, 5%, 7.5%, and 10% that all showed a similar trend to that of 10%. Xiao et al. (In press) perturbed MF, OFL, and TSL $\pm 10\%$ using an OpenSim forward simulation. Their results showed no sensitivity to MF, modest sensitivity to OFL, and significant sensitivity to TSL. In our study we chose to alter the perturbation sizes used by Xiao et al. slightly by using $\pm 5\%$ for OFL and $\pm 15\%$ for TSL since other studies also showed the importance of having accurate values of TSL in relation to other muscle parameters (Delp & Zajac, 1992; Out et al., 1996). To account for the significant variability in an individual's muscle force, we used a large range for MF (-50/+100%) (Buchanan, 1994; Out et al., 1996; Heine et al., 2003; Thelen, 2003; Besier et al., 2009). We were confident that these perturbations were not unreasonably large because instead of arbitrarily using the limits of a predetermined range, we used the EMG-driven model to tune the muscle parameters to subject-specific values.

The EMG-driven model matched the input inverse dynamics well across all subjects with average r^2 values of 0.924 and 0.954 and normalized RMS error of 0.069 and 0.068 for the knee and ankle, respectively. The number of iterations the EMG-driven model performs is set to 100,000 within the simulated annealing algorithm. This value has been shown to allow the model to match experimental data well and

still maintain good predictive ability (Lloyd & Besier, 2003; Shao et al., 2009). Increasing the level of iterations will eventually make the joint moments from forward and inverse dynamics nearly equal. Calibration this exact will make muscle parameters trial specific and not applicable to novel trials. While our study did not use a novel trial to test the validity of the optimized muscle parameters, our r^2 values were consistent with those seen in other studies using the same EMG-driven model (Lloyd & Besier, 2003; Buchanan et al., 2004; Shao et al., 2009; Bassett et al., 2006). This gave us confidence that our optimized values of MF, OFL, and TSL were indicative of in vivo subject-specific muscle parameters.

5.2 Generic Vs. Optimized Muscle Parameters in OpenSim

Two OpenSim forward simulations were performed based on the same experimental data but different muscle parameters. The first involved generic parameters that were scaled to match anthropometric measures, while the second used the optimized parameters from the EMG-driven model. The forward simulation and cost function were identical between both models, meaning any differences seen in muscle force and activation were the result of the altered muscle parameters. For all subjects, muscle activations using optimized muscle parameters showed similar timing but lower magnitude than generically scaled parameters (Figs. 4.2, 4.4, 4.6; dotted and dashed lines). The average ratios of the area under the activation curves for the scaled to optimized OpenSim models showed values greater than 1.0 for all muscles except

the BFSH indicating that optimized activation patterns were lower than for the scaled model (Table 4.5). The decreased activations were consistent with activation patterns seen in self-selected gait studies (Prentice et al., 2001; Thelen & Anderson, 2006; Schmitz et al., 2009; Liikavainio et al., 2010) and more similar in magnitude to normalized EMG activity (Anderson & Pandy, 2001a, Anderson & Pandy, 2001b, Ivanenko et al., 2004, Ricamato & Hidler, 2005; Heintz & Gutierrez-Farewik, 2007; Hubley-Kozey et al., 2009, Kang & Dingwell, 2009). Conversely, average individual muscle force ratios of scaled to optimized modes resulted in ratios less than 1.0 for all muscles except the Sol (Table 4.6). This variation is largely due to the difference in force generating ability from changes in MF. An explanation of how the change in muscle parameters affects the contraction dynamics is important in understanding the differences in muscle forces.

5.2.1 Optimal Fiber Length

In a Hill-type model, muscle force is dependent on the force-length relationship (Zajac, 1989). Therefore, the values of OFL have a direct impact on individual muscle forces since the normalized fiber length is equal to the ratio of fiber length to OFL ($\tilde{l}_m = l_m / l_m^o$). The majority of muscles for the three subjects showed similar patterns but different magnitudes for the normalized fiber lengths between the models using generically scaled and optimized muscle parameters (Fig. 5.1A). Figure 5.1 gives two examples of the normalized fiber length during the stance phase for the Sol and LG.

For the Sol, the normalized fiber length for the scaled model ranged between 0.9 and 1.1, the flat region of the force-length curve (Fig. 2.5), where a change in the fiber length would not have a large effect on the force. Conversely, the optimized model had a normalized fiber length ranging between 0.55 and 0.75 where the force-length curve is steep and slight changes in fiber length would produce a large change in force.

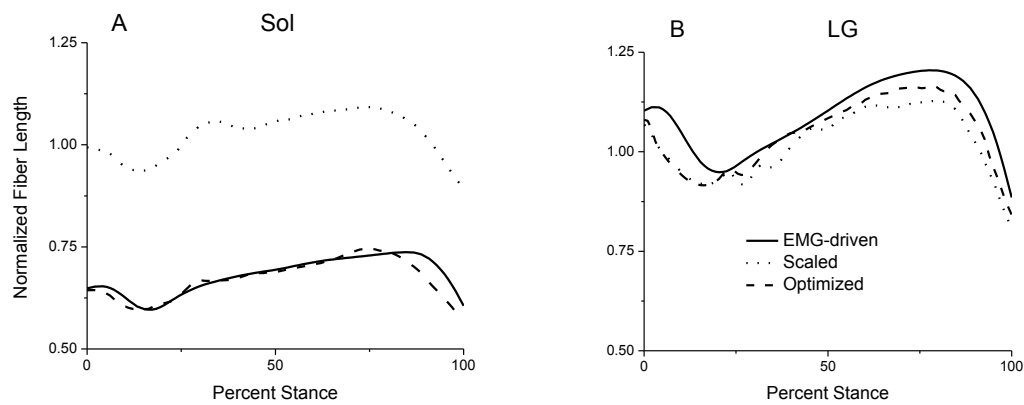


Figure 5.1: Normalized fiber length for the Sol and LG during stance phase for subject 1.

It would be simple to say that the Sol is more sensitive to changes in OFL than LG, where the scaled and optimized normalized fiber lengths operate on similar portions of the force-length curve (Fig. 5.1B), but the level of muscle activation adds a level of complexity. When the activation is 1.0, the active portion of the force-length curve is steepest. Changes in fiber length are magnified on the ascending and descending portions of the active force curve (Fig. 2.5). However, Sol and LG are not

at full activation during the stance phase, and thus operate on active force curves of lower activation where the slope is less steep and changes in fiber length are not as sensitive to muscle force. From Fig. 4.6, it can be seen that the average muscle activation for LG is less than that of Sol, resulting in lower peak normalized muscle force from the force-length curve. Both OFL and muscle activation are coupled together to describe the force-length relationship.

5.2.2 Tendon Slack Length

Several studies show the sensitivity of muscle force to changes in tendon slack length (Delp & Zajac, 1992; Out et al. 1996; Scovil & Ronsky, 2006; Redl et al., 2007; Xiao et al., In press). The TSL defines the crimp region of the tendon force-strain curve. Tendon values below TSL result in no muscle force, and after TSL is reached, the tendon is elongated until the crimp disappears and a linear relationship is achieved. In this study, the average optimized TSL decreased for all muscles from the values in the scaled model (Table 4.2). The SM and vasti muscles showed consistently large decreases across all subjects. A reduction in TSL creates a more compliant (i.e. spring-like) tendon and allows the musculotendon length to operate on a wider range of its force-tension curve (Lieber, 2010). In an isometric contraction where the musculotendon length is maintained, a decrease in fiber length from sarcomere shortening leads to an increase in tendon length. In dynamic tasks like gait, the tendon length-fiber length relationship is more complicated. Griffiths (1991) and Hoffer et al.

(1989) used a surgically implanted length measuring device to show that the muscle fiber length in the MG of a cat shortened even as the musculotendon length increased. In this case, the tendon compliance was such that the tendon accounted for all of the increase in musculotendon length. This discrepancy in results makes it difficult to make a direct relationship between the tendon length and fiber length. Additionally, since tendon length will have an effect on sarcomere length, and thus the muscle fiber force-length curve, OFL will also be affected by the shift in the curve related to tendon stress-strain (Lieber, 2010).

5.2.3 Maximum Isometric Force

Individual muscle force is dependent on the force-velocity and force-length relationships. Force is normalized to MF to allow for a uniform dimensionless comparison between all muscles. Intuitively, MF has a significant effect on muscle force (Eq. 8) and studies have supported this claim (Delp & Zajac, 1992, Buchanan, 1994; Out et al., 1996; Heine et al., 2003; Lloyd & Besier, 2003; Thelen, 2003; Scovil & Ronsky, 2006). It has been shown that there are large variations in MF between subjects (Fukunaga et al., 1997; Zajac et al., 2002; Thelen, 2003) and we accounted for this by setting a large constraint range within the EMG-driven model (-50/+100%). Because we used 3 healthy male subjects, average strength factors, G_f , G_e , reached values close to 2.0 ($F_{\max} = G_{e,f} \cdot F_{\max,est}$) and the force generating ability was nearly doubled (Table 4.3). In other words, if the models using generically scaled and

optimized muscle parameters had similar activation, and force-length and force-velocity relationships, force output from the optimized model would be much higher since the force generating capability is greater than the scaled model. This is evident as the average scaled/optimized force ratios were below 1.0 for all muscles except the Sol.

5.2.4 Summary

The previous discussion highlighted the effect perturbing the muscle parameters OFL, TSL, and MF has on the activation and force output. Previous studies have determined the sensitivity of a musculoskeletal model by perturbing one parameter and calculating the resulting difference in force (Sovil & Ronsky, 2006; Redl et al., 2007, Xiao et al., In press). Because our study perturbed a total of 36 parameters across 12 muscles, it is difficult to quantify the effect of one individual muscle parameter on all other muscle forces. The OpenSim model tracks experimental kinematics, therefore the effect of altering muscle parameters is compensated by both agonist and antagonist muscle forces and activations that will reproduce the same movement pattern. The equations of motion that govern the contraction dynamics help describe how the optimized parameters affect the force and activation output. While there is variation in individual muscle force between the scaled and optimized OpenSim forward simulations, we are confident that the use of subject-specific parameters for MF, OFL, and TSL produces a more accurate result of in vivo measures

because, 1) the validity of subject-specific muscle parameters tuned within the EMG-driven model has been proven (Lloyd & Besier, 2003; Buchanan et al., 2004; Shao et al., 2009; Bassett et al., 2006) and, 2) activation patterns using optimized muscle parameters were more indicative of those seen in normal gait than activation patterns using scaled muscle parameters (Prentice et al., 2001; Thelen & Anderson, 2006; Schmitz et al., 2009; Liikavainio et al., 2010).

5.3 EMG-driven Model Vs. Optimized OpenSim Model

The EMG-driven model and OpenSim have fundamentally different simulation approaches yet we wanted to determine how well estimated individual muscle forces matched between the models. Knee flexors and extensors varied largely in magnitude but showed similar timing of peak forces during stance phase (Figs. 4.3 and 4.5; solid and dashed lines). Ankle muscles showed an improved relationship in terms of timing and magnitude with the largest differences occurring at peak forces (Fig. 4.7). To understand the reasons for the variability in estimated muscle force, we need to highlight the differences in the models.

5.3.1 Activation Dynamics

The EMG-driven model applies Eqs. (1)-(7) to transform EMG to activation while OpenSim estimates a set of muscle excitations that determines activation (Eq. 28, top). While the two models incorporate different muscle parameters that drive the

activation dynamics, both have a time constant accounting for the delay between muscle activation and force production. OpenSim uses global activation and deactivation time constants ($\tau_{\text{act}} = 0.01$; $\tau_{\text{deact}} = 0.04$) for all muscles, while the EMG-driven model tunes the electromechanical delay for each muscle (Corocos et al., 1992; Delp et al., 2007; Buchanan et al., 2004). Subject-specific time delay for each muscle gives an optimized, and likely more accurate, result in relation to the onset of force than the use of generic time constants across subjects.

5.3.2 Contraction Dynamics

The contraction dynamics used in both models, however, applies the same principles of the force-length and force-velocity relationship to the estimation of muscle force. Because the models are using the same values for MF, OFL, and TSL, the effect of contraction dynamics between the models should be negligible. This is evident through inspection of the normalized fiber length. Figure 5.1 shows that the normalized fiber length for the optimized and EMG-driven models for the Sol and LG are virtually the same, thus operating on the same portion of the force-length curve throughout stance phase. Similar relationships occurred for all muscles as well as for muscle fiber velocities.

5.3.3 Cost Function

The most notable difference between the models is the application of the cost functions. The EMG-driven model minimizes the difference between the forward and inverse dynamic joint moment,

$$J = \sum (M_F - M_I)^2 \quad (29)$$

The cost function takes into account the entire time range and individually perturbs the muscle parameters until the moments are matched. The entire forward dynamic loop is rerun for each parameter iteration. The final, subject-specific muscle parameters, along with activation and contraction dynamics, calculate the estimated individual muscle forces (Buchanan et al., 2004).

Similarly, OpenSim uses forward dynamics to determine muscle forces; however the difference arises from the inputs. The EMG-driven model uses filtered EMG as a representation of individual muscular activity and allows the tuned muscle parameters to provide a good estimation of muscle force. Since OpenSim does not incorporate EMG, muscle excitations are used instead to estimate muscle function (Fig. 2.6). First, desired accelerations are calculated using experimental data from inverse kinematics. Static optimization then applies a cost function to the redundant system of equations of motion. The cost function distributes forces across synergistic

muscles at the current time step by minimizing the sum of the square of the normalized muscle forces,

$$J = \sum_{i=1}^{58} \left(\frac{F_{m,i}}{F_{m,i}^o} \right)^2 \quad (30)$$

Muscle excitations are determined such that, when input into the activation and contraction dynamics, the same forces would be produced. Forward dynamics is then run using the excitations to calculate muscle forces at the next time step.

5.3.4 Summary

While both models use fundamentally different approaches to muscle activation dynamics, the majority of differences seen in individual muscle forces is due to the optimization of each cost function. The average ratio of forces from the EMG-driven model to the optimized OpenSim model was less than 1.0 for all muscles except the Sol (Table 4.6). Table 4.3 shows that the EMG-driven model optimized average scale factors to values ranging from 1.705 to 1.977. Increases in MF from scale factors will, in turn, increase values of optimal force at each time step (F_m^o) based on the force-length-velocity relationship. If a uniform scaling was applied across all muscles and the OFL and TSL were held constant, force outputs for the optimized OpenSim model would remain similar because the relative cost of each

muscle would be maintained (Eq. 30). However, since different scale factors were applied across functional muscle groups, the relative cost of each muscle changed. For example, if the Sol (ankle plantar flexor) and the MG (knee flexor, ankle plantar flexor) had scale factors of 2.0 and 1.5, respectively, the relative cost of the Sol would be less, therefore allowing more of the load to be shifted to the Sol to achieve the minimization in the cost function. The issue is confounded, however, by the fact that we also altered OFL and TSL along with MF which will inherently help to determine F_m^o .

The EMG-driven model functions such that the optimized scale factors along with all other muscle parameters used (Table 3.1) can produce a forward dynamic moment that can match the inverse dynamic result. The values used in the single joint EMG-driven model may not be appropriate for an OpenSim model which uses a full musculoskeletal system to reproduce joint kinematics. In particular, the scale factors may lead to values of MF that are too large to produce reasonable muscle forces in OpenSim. Further analysis should refine the physiological boundaries so that muscle forces from the EMG-driven model and the optimized OpenSim model can converge to similar values.

5.4 Net Joint Forces

Despite differences in individual muscle forces, net joint forces show similar timing and magnitude between the OpenSim models, particularly for the ankle (Fig.

4.8; Table 4.7). Scaled and optimized muscle parameter models showed the strongest relationship and, in the case of the ankle, produced net forces that essentially matched. Knee and ankle joint net forces had average r^2 values of 0.92 and 0.98, respectively. This result is not surprising since the computed muscle control algorithm uses the same experimental kinematics, moment arms, and static optimization (i.e. cost function) at each time step. Forward dynamics determines the joint angles and velocities based on the two sets of parameters and are fed back into the forward simulation, affecting the muscle forces at the next time step. The sole difference between the models effecting force output is the change in values used for the muscle parameters MF, OFL, and TSL. Studies have shown that muscles can provide support and accelerate joints that they do not span (Neptune et al., 2001; Liu et al., 2006), therefore slight changes in forces at the ankle could be magnified by muscles that cross the knee as a compensatory strategy to maintain normal gait. While the cost function distributed the individual forces differently across the knee and ankle, it is still encouraging that net forces are similar for both joints.

The EMG-driven and optimized OpenSim models also showed a similar net joint force relationship at the ankle with respect to timing and magnitude. The knee showed greater variability with an average r^2 value of 0.85 as opposed to 0.93 for the ankle. Both models have estimated in vivo muscle function accurately (Lloyd & Besier, 2003; Buchanan et al., 2004; Bassett et al., 2006; Anderson & Pandy, 2001a; Neptune et al., 2001; Anderson & Pandy, 2003; Thelen & Anderson, 2006), thus a

comparison of the two models (EMG-driven and optimized OpenSim) gives us confidence in their ability to perform simulations that converge to similar net joint forces. The two models incorporate identical parameters; however fundamental differences in the models explain the variation in individual muscle forces, which can be addressed by the use of different cost functions. We will address this in the Future Directions section.

5.5 Conclusions

Musculoskeletal modeling has recently become a popular method for researchers to simulate body motion and address the issue of the redundant system of equations. While several studies have reasonably estimated muscle activity, their use of generic parameters provides a limitation which can lead to inaccurate muscle forces and activations. This study incorporated subject-specific parameters optimized in an EMG-driven model to compare the difference in individual muscle forces with those obtained from scaled parameters. We hypothesized that the use of subject-specific parameters would produce a result closer to in vivo values and give better insight into how the neuromuscular system is driven. We made two fundamental comparisons of the models: 1) Comparing muscle forces and activations from an OpenSim model using generically scaled and subject-specific parameters (identical cost function; different muscle parameters) and, 2) Comparing muscle forces between an EMG-

driven and OpenSim model using subject-specific parameters (identical muscle parameters; different cost function).

Muscle activations from subject-specific parameters were less than those from scaled parameters and are more consistent with activations typical of self-selected walking. Individual muscle forces, however, varied across all muscles. Because we perturbed 36 parameters from 12 knee and ankle muscles, it is difficult to quantify effects of individual parameters from such a large scale sensitivity study. While we highlighted the functional relationships and possible effects these changes in parameters could create, a direct cause-and-effect relationship is impossible to determine. It is our belief though, that subject-specific parameters are still important to account for the variability in individual muscle physiology.

Muscle forces from an EMG-driven and optimized OpenSim model also showed large variability. Net joint forces between the models for the knee and ankle, however, showed strong similarity. This is promising because overall joint forces are comparable and the variability seen in individual muscle forces is only due to the distribution of forces by the differences in the cost function.

Applying subject-specific muscle parameters to a forward dynamic simulation can improve functionality and give insight into how muscles are activated. For subjects with pathologic gait (i.e. post-stroke), this information is even more critical as rehabilitation programs can be tailored to target particular deficiencies and return patients to a more active lifestyle.

5.6 Limitations

This study encountered a number of limitations that need to be considered. The most significant limitation comes from the fact that EMG-driven model simulates the muscle function of a single joint, while OpenSim using a full body musculoskeletal model incorporating 58 muscles spanning 23 joints. Since the acceleration of one joint can affect the motion of other body segments, OpenSim can account for this while the EMG-driven model cannot. Similarly, single joint models do not account for biarticular muscles such as the gastrocnemius and rectus femoris. For example, the estimated force of the gastrocnemius creates a moment about both the knee and ankle. The muscle's contribution to the knee moment could impact the effect on the ankle, and in particular, the other plantar flexors. There is likely a direct relationship between gastrocnemius and soleus forces so that the ankle moment is maintained. While this is a limitation of the EMG-driven model, studies have validated their use by accurately estimating muscle forces (Lloyd & Besier, 2003; Buchanan et al., 2004; Bassett et al., 2006; Shao et al., 2009).

To maintain consistency between the models, the muscles used to define the knee and ankle were matched and some muscles (gracilis, sartorius, tibialis posterior) were eliminated. In true gait these muscles carry a force, but Xiao et al. (In press) showed that the effect of smaller muscles is negligible to the overall distribution of forces in the lower extremity.

Subject-specific muscle parameters were estimated using the EMG-driven model for only the ankle and knee. Perturbing the values of MF, OFL, and TSL changes the force generating capability for each muscle and, by not accounting for hip muscles, the compensatory strategy used to optimize the cost function could directly impact the distribution of forces. The intent of this study, however, was to analyze the effect of subject-specific parameters on the lower extremities during gait, therefore muscle forces seen at the hip and all other joints in this study should not be generalized to the entire population.

There has also been concern as to whether gait parameters from overground walking can be reproduced using a split-belt treadmill. A deviation from normal gait patterns could affect how muscles are activated and their resulting forces. Studies have shown however, that with appropriate adaptation time, similar kinematics can be reproduced (Riley et al., 2007; Zeni & Higginson, 2010).

Finally, our study only included three healthy young adults. While a larger population would add to the strength of these comparisons and hopefully converge on similar trends, we believe that the variability seen in muscle function is the product of how the cost function distributes forces based on the global use of subject-specific parameters rather than the population size.

5.7 Future Directions

This thesis looked at how musculoskeletal forward simulations could be improved with the use of subject-specific parameters in a healthy population. It is our hope that this study can be extended to pathologic gait. It is known that muscle physiology changes in subjects post-stroke. Studies using forward simulation have already been proven to accurately reproduce experimental kinematics seen in post-stroke subjects; however, these incorporated scaled muscle parameters (Higginson et al., 2006; Xiao & Higginson, In press). EMG-driven models have also been used with pathologic gait to account for differences in muscle parameters (Shao et al., 2009). By incorporating subject-specific parameters from post-stroke gait into an OpenSim forward simulation, variations in muscle force can highlight functional deficiencies for a particular individual. Such information can be used clinically to assist in the design of treatment interventions that address specific impairments and improve gait speed in patients post-stroke.

Different cost functions should also be tested within the CMC algorithm of OpenSim since the cost function in human gait is not well established (Glitsch & Bauman, 1997; Pedotti et al., 1978; Kaufman et al., 1991; Bean et al. 1988; Crowninshield & Brand, 1981). While OpenSim currently uses the minimization of squared normalized muscle forces, other studies have minimized the metabolic energy (Anderson & Pandy, 2001a; Anderson & Pandy, 2001b) and the difference between experimental and simulated motions (Neptune et al., 2001; Zajac et al., 2003;

Higginson et al., 2006). A cost function minimizing the square of sum of muscle stresses could add an additional level of specificity. Muscle stress is the maximum isometric force divided by the physiological cross-sectional area ($\sigma = F_m^o / PCSA$). PCSA can be determined experimentally through imaging techniques such as magnetic resonance imaging (MRI), ultrasound, and CT scans. Research within our lab has already began to use MRI to determine muscle volumes for both healthy and stroke subjects which we hope can provide accurate measures of muscle morphology that will give better estimates of muscle function.

OpenSim muscle forces show significant spikes resulting from the static optimization in the CMC algorithm. The cost function could also be improved to include constraints or multiple cost functions that work over different ranges of the stance phase. For example, if it is known that TA functions in the first 20% of stance as the foot is flattened to the ground, and the last 10% before toe-off, two cost functions could be defined to account for the ranges when the muscle is active and inactive. This would eliminate unusual peaks in muscle force when activation is very low.

The long term goal of this study is to implement the EMG-driven model within OpenSim. The current muscle activation dynamics could be replaced by the set of equations that transforms filtered EMG to muscle activation. This would greatly improve the utility of an OpenSim forward simulation because muscle activation could be based on actual muscle activity instead of estimations from muscle excitations.

REFERENCES

- Anderson FC, Pandy MG. Dynamic optimization of human walking. *Journal of Biomechanical Engineering*, 2001a, 123, 381-390.
- Anderson FC, Pandy MG. Static and dynamic optimization solutions for gait are practically equivalent. *Journal of Biomechanics*, 2001b, 34; 153-161.
- Anderson FC, Pandy MG. Individual muscle contributions to support in normal walking. *Gait & Posture*, 2003, 17; 159-169.
- Arnold AS, Salinas S, Asakawa DJ, Delp SL. Accuracy of muscle moment arms estimated from MRI-based musculoskeletal models of the lower extremity. *Computer Aided Surgery*, 2000, 5; 108-119.
- Bassett DN, Gardinier JD, Manal KT, Buchanan TS. Estimation of muscle forces about the ankle during gait in healthy and neurologically impaired subjects. In: Begg R, Palaniswami M. *Computational Intelligence for Movement Sciences: Neural Networks and Other Emerging Techniques*. Hershey, PA, Idea Group, 2006; 320-347
- Bean JC, Chaffin DB, Schultz AB. Biomechanical model calculation of muscle contraction forces: A double linear programming method. *Journal of Biomechanics*, 1988, 21; 59-66.
- Besier TF, Fredericson M, Gold GE, Beaupré GS, Delp SL. Knee muscle forces during walking and running in patellofemoral pain patients and pain-free controls. *Journal of Biomechanics*, 2009, 42; 898-905.
- Buchanan TS. Evidence that maximum muscle stress is not a constant: differences in specific tension in elbow flexors and extensors. *Medical Engineering & Physics*, 1994, 17; 529-536.
- Buchanan TS, Shreeve DA. An evaluation of optimization techniques for the prediction of muscle activation patterns during isometric tasks. *Journal of Biomechanical Engineering*, 1996, 118; 565-574.

- Buchanan TS, Lloyd DG, Manal K, Besier TF. Neuromusculoskeletal modeling: Estimation of muscle forces and joint moments and movements from measurements of neural command. *Journal of Applied Biomechanics*, 2004, 20; 367-395.
- Corcos DM, Gottlieb GL, Latash ML, Almeida GL, Agarwal GC. Electromechanical delay: an experimental artifact. *Journal of Electromyography and Kinesiology*, 1992, 2; 59-68.
- Crowninshield RD, Brand RA. A physiologically based criterion of muscle force reduction in locomotion. *Journal of Biomechanics*, 1981, 14; 793-801.
- Davy DT, Audu ML. A dynamic optimization technique for predicting muscle forces in the swing phase of gait. *Journal of Biomechanics*, 1987, 20; 187-201.
- Delp SL, Loan JP, Hoy MG, Zajac FE, Topp EL, Rosen JM. An interactive graphics-based model of the lower extremity to study orthopaedic surgical procedures. *IEEE Transactions on Biomedical Engineering*, 1990, 37; 757-767.
- Delp SL, Zajac FE. Force and moment generating capacity of lower extremity muscles before and after tendon lengthening. *Clinical Orthopaedics and Related Research*, 1992, 284; 247-259.
- Delp SL, Anderson FC, Arnold AS, Loan P, Habib A, John CT, Guendelman E, Thelen DG. OpenSim: open-source software to create and analyze dynamic simulations of movement. *IEEE Transactions of Biomedical Engineering*, 2007, 11; 1940-1950.
- Epstein M, Herzog W. *Theoretical Models of Skeletal Muscle*, Wiley, New York, NY, USA, 1998.
- Fukunaga T, Kawakami Y, Kuno S, Funato K, Fukashiro S. Muscle architecture and function in humans. *Journal of Biomechanics*, 1997, 30; 457-63.
- Garner BA, Pandy MG. Estimation of musculotendon properties in the human upper limb. *Journal of Biomedical Engineering*, 2003, 31; 207-220.
- Glitsch U, Baumann W. The three-dimensional determination of internal loads in the lower extremity. *Journal of Biomechanics*, 1997, 30; 1123-1131.
- Goffe WL, Ferrier GD, Rogers J. Global optimization of statistical functions with simulated annealing. *Journal of Econometrics*, 1994, 60; 65-99.

- Gordon AM, Huxley AF, Julian FJ. The variation in isometric tension with sarcomere length in vertebrate muscle fibers. *Journal of Physiology (London)*, 1966, 184; 170-192.
- Gregor RJ, Komi PV, Browning RC, Jarvinen M. A comparison of the triceps surae and residual muscle moments at the ankle during cycling. *Journal of Biomechanics*, 1991, 24; 287-297.
- Griffiths RI. Shortening of muscle fibers during stretch of the active cat medial gastrocnemius muscle: the role of tendon compliance. *Journal of Physiology (London)*, 1991, 436; 219-236.
- Heine R, Manal K, Buchanan TS. Using Hill-type muscle models and EMG data in a forward dynamic analysis of joint moment: evaluation of critical parameters. *Journal of Mechanics in Medicine and Biology*, 2003, 3; 169-186.
- Heintz S, Gutierrez-Farewik EM. Static optimization of muscle forces during gait in comparison to EMG-to-force processing approach. *Gait & Posture*, 2007, 26; 279-288.
- Higginson JS, Zajac FE, Neptune RR, Kautz SA, Delp SL. Muscle contributions to support during gait in an individual with post-stroke hemiparesis. *Journal of Biomechanics*, 2006, 39; 1769-1777.
- Hill AV. The heat of shortening and the dynamic constant of muscle. *Proceedings of the Royal Society of London Series B*, 1938, 126; 136-195.
- Hoffer JO, Caputti AA, Pose IE, Griffiths RI. Roles of muscle activity and load on the relationship between muscle spindle length and whole muscle length in the freely walking cat. *Progress in Brain Research*, 1989, 80; 75-85.
- Hubley-Kozey CL, Hill NA, Rutherford DJ, Dunbar MJ, Stanish WD. Co-activation differences in lower limb muscles between asymptomatic controls and those with varying degrees of knee osteoarthritis during walking. *Clinical Biomechanics*, 2009, 24; 407-414.
- Huijing PA. Important experimental factors for skeletal muscle modeling: nonlinear changes of muscle length force characteristics as a function of degree of activity. *European Journal of Morphology*, 1996, 34; 47-54.
- Huxley AF. Muscle structure and theories of contraction. *Progress in Biophysical Chemistry*, 1958, 7; 255-318.

- Ivanenko YP, Popple RE, Lacquaniti F. Five basic muscle activation patterns account for muscle activity during human locomotion. *Journal of Physiology*, 2004, 556; 267-282.
- Kang HG, Dingwell JB. Dynamics and stability of muscle activations during walking in healthy young and older adults. *Journal of Biomechanics*, 2009, 42; 2231-2237.
- Kaufman KR, An KN, Litchy WJ, Chao EY. Physiological prediction of muscle forces-I. Theoretical formulation. *Neuroscience*, 1991, 40; 781-792
- Komi PV, Salonen M, Jarvinen M, Kokko O. In vivo registration of Achilles tendon forces in man. I. Methodological development. *International Journal of Sports Medicine*, 1987, 7; 3-8.
- Komi PV. Relevance of in vivo force measurements to human biomechanics. *Journal of Biomechanics*, 1990, 23; 23-34.
- Komi PV, Fukashiro S, Jarvinen M. Biomechanical loading of Achilles tendon during normal locomotion. *Clinical Sports Medicine*, 1992, 11; 521-531.
- Kuo AD. A least-squares estimation to improving the precision of inverse dynamics computations. *Journal of Biomechanical Engineering Transactions of the ASME*, 1998, 120; 148-159.
- Lieber RL. Skeletal muscle architecture: implications for muscle function and surgical tendon transfer. *Journal of Hand Therapy*, 1993, 6; 105-113.
- Lieber RL, Loren GJ, Frieden J. In vivo measurements of human wrist extensor muscle sarcomere length changes. *Journal of Neurophysiology*, 1994, 71; 874-881.
- Lieber RL. Skeletal Muscle Structure, Function, and Plasticity. *The Physiological Basis of Rehabilitation: Third Edition*. Baltimore, MD: Lippincott Williams & Williams, 2010.
- Liikavainio T, Bragge T, Hakkarainen M, Karjalainen PA, Arkoski JP. Gait and muscle activation changes in men with knee osteoarthritis. *The Knee*, 2010, 17; 69-76.

- Liu MQ, Anderson FC, Pandy MG, Delp SL. Muscles that support the body also modulate forward progression during walking. *Journal of Biomechanics*, 2006, 39; 2623-2630
- Lloyd DG, Buchanan TS. A model of load sharing between muscles and soft tissues at the human knee during static tasks. *Journal of Biomechanical Engineering*, 1996, 118; 367-376.
- Lloyd DG, Besier TF. An EMG-driven musculoskeletal model for estimation of the human knee joint moments across varied tasks. *Journal of Biomechanics*, 2003, 36; 765-776.
- Manal K, Gonzalez RV, Lloyd DG, Buchanan TS. A real-time EMG driven virtual arm. *Computers in Biology and Medicine*, 2002, 32; 25-36.
- Manal K, Buchanan TS. A one-parameter neural activation to muscle activation model: estimating isometric joint moments from electromyograms. *Journal of Biomechanics*, 2003, 36; 1197-1202.
- Milner-Brown HS, Stein RB, Yemm R. Changes in firing rate of human motor units during linearly changing voluntary contractions. *Journal of Physiology (London)*, 1973, 228; 371-390.
- Mungiole M, Martin PE. Estimating segment inertial properties: comparison of magnetic resonance imaging with existing methods. *Journal of Biomechanics*, 1990, 23; 1039-1046.
- Narici M, Maffulli N, Maganaris C. Aging in human muscles and tendons. *Disability and Rehabilitation*, 2008; 1-7.
- Neptune RR, Hull ML. Evaluation of performance criteria for simulation of submaximal steady-state cycling using a forward dynamic model. *Journal of Biomechanical Engineering*, 1998, 120, 3; 334-341.
- Neptune RR. Optimization algorithm performance in determining optimal controls in human movement analyses. *Journal of Biomechanical Engineering*, 1999, 121; 249-252.
- Neptune RR, Kautz SA, Zajac FE. Contributions of the individual ankle plantar flexors to support, forward progression and swing initiation during swing. *Journal of Biomechanics*, 2001, 34; 1387-1398.

- Out L, Vrikkotte TG, van Soest AJ, Bobbert MF. Influence of the parameters of a human triceps surae muscle model on the isometric torque-angle relationship. *Journal of Biomechanics*, 1996, 118; 17-25.
- Pedotti A, Krishnan VV, Stark L. Optimization of muscle-force sequencing in human locomotion. *Mathematical Biosciences*, 1978, 38; 57-76.
- Piazza SJ, Delp SL. The influence of muscles on knee flexion during the swing phase of gait. *Journal of Biomechanics*, 1996, 29, 723-733.
- Piazza SJ. Muscle-driven forward dynamic simulations for the study of normal and pathological gait. *Journal of NeuroEngineering and Rehabilitation*, 2006, 3; 5.
- Prentice SD, Patla AE, Stacey DA. Artificial neural network model for the generation of muscle activation patterns for human locomotion. *Journal of Electromyography and Kinesiology*, 2001, 11; 19-30.
- Redl C, Gfoehler M, Pandy MG. Sensitivity of muscle force estimates to variations in muscle-tendon properties. *Human Movement Science*, 2007, 26, 306-319.
- Ricamato AL, Hidler JM. Quantification of the dynamic properties of EMG patterns during gait. *Journal of Electromyography and Kinesiology*, 2005, 15; 384-392.
- Riley PO, Paolini G, Della Croce U, Paylo KW, Casey Kerrigan DC. A kinematic and kinetic comparison of overground and treadmill walking in healthy subjects. *Gait & Posture*, 2007, 26; 17-24.
- Rugg SG, Gregor RJ, Mandelbaum BR, Chiu L. In vivo moment arm calculations at the ankle using magnetic resonance imaging. *Journal of Biomechanics*, 1990, 23; 495-501.
- Schmitz A, Silder A, Heiderscheit B, Mahoney J, Thelen DG. Differences in lower-extremity muscular activation during walking between healthy older and young adults. *Journal of Electromyography and Kinesiology*, 2009, 19; 1085-1091.
- Schutte LM. Using musculoskeletal models to explore strategies for improving performance in electrical stimulation-induced leg cycle ergometry, *PhD Thesis*, 1993, Stanford University.
- Schutte LM, Rodgers MM, Zajac FE. Improving the efficacy of electrical stimulation induced leg cycle ergometry: an analysis based on a dynamic musculoskeletal model. *IEEE Transactions on Rehabilitation Engineering*, 1993b, 1; 109-124.

- Scott SH, Winter DA. A comparison of three muscle pennation assumptions and their effect on isometric and isotonic force. *Journal of Biomechanics*, 1991, 24; 163-167.
- Seireg A, Arvikar RJ. A mathematical model for evaluation of forces in lower extremities of the musculo-skeletal system. *Journal of Biomechanics*, 1973, 6; 313-326.
- Shao Q, Bassett DN, Manal KT, Buchanan TS. An EMG-driven model to estimate muscle forces and joint moments in stroke patients. *Computers in Biology and Medicine*, 2009, 39; 1083-1088.
- Thelen DG, Schultz AB, Fassois SD, Ashton-Miller JA. Identification of dynamic myoelectric signal-to-force models during isometric lumbar muscle contractions. *Journal of Biomechanics*, 1994, 27; 907-919.
- Thelen DG, Anderson FC, Delp SL. Generating dynamic simulations of movement using computed muscle control. *Journal of Biomechanics*, 2003, 36; 321-328.
- Thelen DG, Anderson FC. Using computed muscle control to generate forward dynamic simulations of human walking from experimental data. *Journal of Biomechanics*, 2006, 39; 1107-1115.
- Woittiez RD, Huijing PA, Boom HB, Rozendal RH. A three-dimensional muscle model: a quantified relation between form and function of skeletal muscles. *Journal of Morphology*, 1984, 182; 95-113.
- Woods JJ, Bigland-Ritchie B. Linear and non-linear surface EMG/force relationships in human muscles. An anatomical/functional argument for the existence of both. *American Journal of Physical Medicine*, 1983, 62; 287-299.
- Xiao M, Zeni J, Higginson JS. Sensitivity of predicted muscle force in forward simulation of normal walking. *Journal of Applied Biomechanics*, In press.
- Xiao M, Higginson JS. Individual muscle contributions to joint acceleration in post stroke hemiparetic gait. In Press.
- Yamaguchi GT, Sawa AGU, Moran DW, Fessler MJ, Winters JM. A survey of human musculotendon actuator parameters. *Multiple Muscle Systems: Biomechanics and Movement Organization*, Springer-Verlag, New York, NY, USA, 1990.

- Zahalak GI. A comparison of the mechanical behavior of the cat soleus muscle with a distribution-moment model. *Journal of Biomechanical Engineering*, 1986, 108; 131-140.
- Zahalak GI. The two-state cross-bridge model of muscle is an asymptotic limit of multi-state models. *Journal of Theoretical Biology*, 2000, 204; 67-82.
- Zajac FE. Muscle and tendon: Properties, models, scaling, and application to biomechanics and motor control. *Critical Reviews in Biomedical Engineering*, 1989, 17; 359-411.
- Zajac FE. Muscle coordination of movement: a perspective. *Journal of Biomechanics*, 1993, 26; 109-124.
- Zajac FE, Neptune R, Kautz SA. Biomechanics and muscle coordination of human walking. Part I: Introduction to concepts, power, transfer, dynamics, and simulations. *Gait and Posture*, 2002, 16; 215-232.
- Zajac FE, Neptune R, Kautz SA. Biomechanics and muscle coordination of human walking. Part II: lessons from dynamical simulations and clinical implications. *Gait and Posture*, 2003, 17; 1-17.
- Zeni JA, Higginson JS. Gait parameters and stride-to-stride during familiarization to walking on a split-belt treadmill. *Clinical Biomechanics*, 2010, 25; 383-386.